International Journal of Pharmaceutics 673 (2025) 125417

Contents lists available at ScienceDirect

International Journal of Pharmaceutics

journal homepage: www.elsevier.com/locate/ijpharm

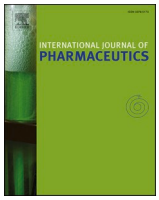

Delivery of Fenofibrate to Ocular Tissues using 2-Hydroxypropyl-β-cyclodextrin-Based Micelles

Butsabarat Klahan [a,*], Niall J. O'Reilly [a], Hakon Hrafn Sigurdsson [b], Anuj Chauhan [c], Satu Mering [d], Laurence Fitzhenry [a,*]

[a] Ocular Therapeutics Research Group (OTRG), Pharmaceutical and Molecular Biotechnology Research Centre (PMBRC), South East Technological University (SETU), X91 K0EK Waterford, Ireland
[b] Faculty of Pharmaceutical Sciences, University of Iceland, Hofsvallagata 53, IS-107 Reykjavik, Iceland
[c] Chemical and Biological Engineering Department, Colorado School of Mines, Golden, CO 80401, USA
[d] Experimentica Ltd. Global Headquarters and Labs, Microkatu 1, P.O. Box 1199 70211 Kuopio, Finland

ARTICLE INFO

Keywords:
Fenofibrate
PF127
Micelles
Poly(pseudo)rotaxanes
2-HPβCD
Mixed micelles

ABSTRACT

Age-related macular degeneration and diabetic retinopathy are the main diseases that cause vision impairment. The standard treatment for this condition is the intravitreal injection of anti-vascular endothelial growth factor agents, which cause several side effects to the eye after injection. Topical administration would be a more effective method, but the ocular layers act as barriers to drug diffusion. In this research, we presented the preparation and characterization of poly(pseudo)rotaxanes (PPRs) containing 2-hydroxypropyl-β-cyclodextrin (2-HPβCD), Pluronic® F127 (PF127) and Soluplus® to enhance the solubility of fenofibrate (FEB), a poorly water-soluble drug, for potential application in ocular drug delivery. The FEB-loaded micelles and PPRs were investigated using DLS, ^{1}H NMR and XRD techniques, which demonstrated that FEB could be encapsulated into both micelles and PPRs with small particle sizes (7–67 nm). The inclusion complex between FEB and 2-HPβCD was observed, as evidenced by a high stability constant ($K_{1:1}$) and the shift in proton positions (^{1}H NMR) within the hydrophobic cavity of 2-HPβCD in the FEB-loaded PPR formulations. Moreover, ^{1}H NMR demonstrated structural modifications involving the PF127/ Soluplus® copolymers and proton shifts at the exterior wall of 2-HPβCD in the FEB-loaded PPR formulations, supporting the interactions between the copolymers and 2-HPβCD. The XRD pattern of free FEB compound, indicating its crystalline structure, whereas the drug-loaded PPRs (PF127/Soluplus®/2-HPβCD) showed an amorphous phase with a single broadband without a sharp diffraction peak, suggesting the transformation of the FEB drug from the crystalline to the amorphous state. Subsequently, the solubility enhancement of FEB in the prepared formulations was evaluated and found that the addition of 2-HPβCD to the mixed PF127/Soluplus® micelles had a 910-fold increase in FEB solubility compared to the intrinsic solubility of the FEB (0.34 ± 0.0011 μg/mL), indicating a synergistic effect of 2-HPβCD in drug solubility enhancement. *Ex vivo* permeation across porcine eyes revealed that FEB-loaded PPRs helped FEB to cross the scleral tissue with FEB permeation levels varying from 0.27 to 4.25 μg/cm^2. Mathematical modelling based on Fick's law was employed to explain the transportation of FEB-loaded micelles or PPRs across the scleral tissue and to calculate effective diffusivity (D_{eff}). Thus, this study highlights the potential application of PPRs as an effective drug delivery system for eye disease treatments and the importance of mathematical modelling in understanding drug permeation mechanisms.

1. Introduction

Fenofibrate (FEB) is a prodrug of fenofibric acid and a peroxisome proliferator-activated receptor alpha (PPARα) agonist, which is a ligand-activated transcription regulator expressed in multiple organs, including the retina (Qiu et al., 2017). In clinical trials, FEB displayed a therapeutic effect on the treatment of eye diseases such as diabetic retinopathy (DR) and neovascular age-related macular degeneration (AMD)

* Corresponding authors at: Ocular Therapeutics Research Group (OTRG), Pharmaceutical and Molecular Biotechnology Research Centre (PMBRC), South East Technological University (SETU), Cork Road, Waterford City, Co. Waterford X91 K0EK, Ireland.
E-mail addresses: butsabarat.klahan@postgrad.setu.ie (B. Klahan), Laurence.Fitzhenry@setu.ie (L. Fitzhenry).

https://doi.org/10.1016/j.ijpharm.2025.125417
Received 27 September 2024; Received in revised form 26 February 2025; Accepted 26 February 2025
Available online 27 February 2025

(Qiu et al., 2017). Moreover, it offers advantages over anti-VEGF agents including low cost, fewer side effects, and neuroprotective effects caused by a reduction of reactive oxygen species and decreased cellular apoptosis under oxidative stress (Chen et al., 2007; Ibáñez et al., 2023; Hsu et al., 2020). However, FEB has some characteristics that limit its therapeutic use. For instance, the solubility of FEB in water is very low (<0.5 μg/mL in water, log P = 5.24), and small molecular weight drugs are very difficult to get into the vitreous, preventing topically applied drugs from reaching the target sites in the posterior eye segments (Wang et al., 2021; Lee et al., 2020). Therefore, various strategies have been explored to increase FEB solubility and stability, prolong the residence time of FEB in the eye, and enhance FEB permeability across ocular tissues (e.g., the cornea and sclera) (Pandit et al., 2023; Hanaguri et al., 2022; Huang et al., 2021; Khin et al., 2022). To date, multiple technologies and materials have been investigated to deliver FEB in a highly dispersed form to improve its bioavailability for ocular drug delivery (OcDD), including nanomicelles and drug/cyclodextrin (CD) complexes (Qiu et al., 2019; Elsaid et al., 2016; Sousa et al., 2017; Kelly et al., 2018).

CDs are toroidal oligosaccharides with a hydrophilic outer surface (a host molecule) and a lipophilic inner surface that are capable of forming inclusion complexes with a guest molecule including hydrophobic drugs and poly(pseudo)rotaxane (PPR) structure, a type of molecular architecture mechanically interlocked and consisting of polymer backbones connected through cyclic molecules. As a result, they can enhance drug permeation across biological barriers and deliver the drug to the targeted site (Khin et al., 2022; Mahesh et al., 2020; Nedelcu et al., 2022).

In terms of OcDD, CDs are added to increase the solubility of the drug in polymeric micelles (PMs) and thus have been shown to effectively enhance permeation and reduce cytotoxicity when in contact with the cornea (Nabih Maria et al., 2017). Jansook *et al.* studied encapsulating dexamethasone (DEX) and amphotericin B (AmB) in Pluronic® F127 (PF127) micelles and PPRs for eye inflammation treatment (Jansook et al., 2016). In their study, the eye drop formulations consisted of PF127 with γ-CD and 2-hydroxypropyl-γ-CD (2-HPγCD) and 1.5% (w/v) DEX and 0.15% (w/v) AmB loading was prepared. Results found that the drug solubility was 2-fold higher in PF127/γ-CD/2-HPγCD PPRs (10–200 nm) with 60/40 of γ-CD/2-HPγCD mixture compared to PPRs with 80/20 of γ-CD/2-HPγCD mixture (9.73 and 0.115 mg/mL for DEX and AmB, respectively), indicating a synergistic effect of the inclusion complex between the drug and larger hydrophilic portion of 2-HPγCD. Furthermore, an *in vitro* permeation study revealed a slower drug permeation profile of the PPR formulation when increasing PF127 content from 2.5% to 5% (w/v), which caused by an increase in complex aggregates of the copolymers. The apparent permeation coefficient (P_{app}) of DEX reduced from 2.5 x 10^{-6} to 1.7 x 10^{-6} cm/s, whereas the P_{app} for AmB decreased from 0.1 x 10^{-6} to 0.07 x 10^{-6} cm/s (Jansook et al., 2016). Similarly, Sayed and coworkers developed β-CD consolidated micellar dispersions (CMD) composed of β-CD, Pluronic® F-108, Pluronic® P84, and polyethylene oxide (PEO), which could self-assemble into CMDs to solubilize the hydrophobic drug, itraconazole, by a melt dispersion technique (Sayed et al., 2018). The optimized CMD formulation had a zeta potential (ZP) of −17.4 mV and a 4.1% solubilization efficiency, with a 2-fold higher permeation in rabbit cornea than the drug suspension (0.30 mg/cm^2). Therefore, these studies demonstrated the advantages of using triblock copolymers in combination with CDs to form soluble PPR complexes which results in enhanced encapsulation efficiency (EE) aqueous solubility and therapeutic activity of the drug (Pignatello et al., 2022; Feng et al., 2020; Alvarez-Rivera et al., 2016; Wang et al., 2017; Dehvari et al., 2016; Pepić et al., 2010).

Mathematical models can expedite the design process and enhance understanding for researchers of the mechanism of action in OcDD systems by combining computational modelling with experimental study. Compartment models and Fick's law of diffusion are utilized as theoretical frameworks for investigating the process of drug permeation across biological membranes. Compartment models separate complicated biological systems into different compartments corresponding to different physiological barriers. This can help with the prediction of both pharmacokinetics and pharmacodynamics of drugs as well as drug behaviour over time. In addition, researchers can gain insights into factors influencing transport and bioavailability of the drug permeation by using mathematical modelling and applying Fick's equations, which describe the rate of diffusion of a substance across a barrier following on factors such as concentration gradient, barrier thickness and diffusion coefficient (German et al., 2023; Worakul and Robinson, 1997; Agrahari et al., 2016; Setapa et al., 2020). In terms of experimental study, transportation of a molecule across biological membranes such as the cornea or conjunctiva in both *in vitro* and *ex vivo* permeation studies is commonly characterized by the P_{app} where the permeability is measured by mounting the membrane in a diffusion chamber that includes the donor and receiver chambers (Veit et al., 2022; Lorenzo-Veiga et al., 2019; Pescina et al., 2019). Pescina *et al.* conducted a study to evaluate the permeability profiles of three different drugs, including DEX, cyclosporine-A (CsA), and econazole nitrate, which were encapsulated within the PMs prepared using TPGS (D-α-Tocopheryl polyethylene glycol 1000 succinate)/PF127 micelles (Pescina et al., 2019). Their study found that 12 nm-sized DEX-loaded TPGS micelles (P_{app} = 3.26 × 10^{-6} cm/s) had higher drug permeation across porcine conjunctiva compared to the CsA (P_{app} = 0.46 × 10^{-6} cm/s). In contrast, there was no econazole nitrate drug penetration across the conjunctival tissue of the porcine eyes. In another study, Toffoletto *et al.* developed a mathematical model to predict the drug concentration over time in different eye compartments by applying soft contact lenses to the cornea and studying drug permeation across different tissues, including tears, sclera, retina, aqueous humor, and vitreous humor, to the posterior segment of the eye (Toffoletto et al., 2023). Their mathematical model provided a better understanding of drug transportation over time in different tissues, which was beneficial for clinical use in the estimation of the drug dose. Thus, comparing and analyzing the P_{app} values obtained from each formulation could help the researchers be able to identify the most promising candidates of the formulations for further development as an OcDD system.

Therefore, the aim of this paper was to evaluate the efficacy of CD-micelle mixed systems formed by 2-HPβCD and copolymers of PF127 and/or Soluplus® as a vehicle to enhance the solubility and permeability of FEB across the porcine eyes for OcDD. This study focused on only FEB drug due to its hydrophobic and anti-VEGF properties, which makes it a promising candidate for OcDD system targeting vascular-related conditions, including AMD. Moreover, a key aspect of this study was to explore how specific formulations, such as supramolecular structure, could enhance the solubility and bioavailability of FEB. This paper also highlighted the integration of various characterization techniques, including DLS, ^{1}H NMR, and XRD to elucidate the PPR structures based on 2-HPβCD and PF127/Soluplus® micelles, which have not been extensively investigated before. Additionally, another goal focused on utilizing the data of drug permeation across the excised cornea and sclera of the porcine eyes to develop an understanding of the mechanism of transport of the FEB-loaded micelles, mixed micelles, and PPRs across the epithelia based on Fick's law, in which this finding has not been previously studied in any other research works.

2. Materials and methods

2.1. Materials

Pluronic F127 triblock copolymer (PF127, mw:12600 g/mol) was purchased from Sigma Aldrich (Arklow, Ireland). Phosphate buffered saline (PBS) tablets (pH 7.4) from Sigma Aldrich (Arklow, Ireland) were used for the preparations of phosphate buffer solutions. One tablet was dissolved in 200 mL of MilliQ water to prepare the PBS solution to yield 0.01 M potassium chloride and 0.137 M sodium chloride. Acetonitrile (ACN) and ortho-phosphoric acid (85%) were all purchased from Sigma

Aldrich (Missouri, USA). Soluplus® (mw:118000 g/mol) from BASF (Ludwigshafen, German) and propan-2-yl 2-[4-(4-chlorobenzoyl)phenoxy]-2-methylpropanoate (fenofibrate, FEB, >98.0%, GC grade, mw:360.83 g/mol, melting point 81 °C) from TCI EUROPE N.V. (Zwijndrecht, Belgium) in powdered form were used as received without further purification. 2-hydroxypropyl-β-cyclodextrin (2-HPβCD, DS 4.2; mw:1380 g/mol) was provided from Janssen Pharmaceutica (Geel, Belgium). MilliQ water (Millipore, Billerica, MA resistivity = 18.2 MΩ. cm) was used to prepare all solutions.

2.2. Solubility studies of fenofibrate in aqueous copolymer solutions

An accurately weighed excess amount of FEB (~8–9 mg) was added to 2 mL of the aqueous solutions of copolymers (PF127, Soluplus®) at concentrations of 0.01, 0.1, 1, 3, 5, 7 and 14% (w/v) in PBS (pH 7.4). The mixtures were stirred for 2 days at 25 ± 3 °C to reach equilibrium. After that, the samples were taken and filtered using a 0.2 μm PTFE membrane filter. The filtered samples were diluted with 50% ACN prior to analysis by HPLC at a wavelength of 285 nm, equipped with a Kinetex® 5 μm C18 150 × 4.6 mm column. ACN:0.1% (v/v) phosphoric acid (75:25% (v/v)) was used as the mobile phase with a flow rate of 1.2 mL/min. The FEB concentration was calculated from a standard calibration curve. The experiment was repeated three times, and the results presented as the mean ± standard deviation (SD).

2.3. Preparation of fenofibrate-loaded micelles and mixed micelles

The single micelles were prepared by dissolving 150 mg of either PF127 or Soluplus® polymers in 3 mL PBS solution (pH 7.4, 5% (w/v)). Whereas the mixed micelles were prepared by directly dissolving PF127 (150 mg) and Soluplus® (150 mg) together in 3 mL of PBS solution (pH 7.4), resulting a final total polymer concentration of 100 mg/mL (10% (w/v)). The formulations were then placed on the magnetic stirrer with stirring at 370 rpm for 24 h at room temperature. 10 mg of FEB was then added into 3 mL polymer solutions with continuous stirring for an additional two days before filtering with 0.22 μm cellulose filters to remove any unincorporated FEB. The final concentration of the dissolved FEB were 0.13 ± 0.06 mg/mL in the PF127 micelles, 0.05 ± 0.02 mg/mL in Soluplus® micelles, and 0.23 ± 0.08 mg/mL in the mixed PF127/Soluplus® micelles (Table 1). The filtered solution was collected for dynamic light scattering (DLS) without dilution and then diluted with 50% ACN for HPLC analysis. The experiment was repeated three times, and the results were presented as the mean ± SD.

2.4. Preparation of poly(pseudo)rotaxanes

Preparation of poly(pseudo)rotaxanes (PPRs) was carried out by combining powder Compound A (copolymers as listed above) and Compound B (2-HPβCD) in 3 mL of PBS (pH 7.4). For Compound A, PF127 or Soluplus® was added directly as a powder to 3 mL of PBS (pH 7.4) at a concentration of 5% (w/v) with stirring until fully dissolved, observing a clear solution. Compound B was then added at a concentration of either 7.5% or 15% (w/v), and the mixture was stirred at 370 rpm for 24 h at room temperature to form the PPRs. Subsequently, 10 mg of FEB was added to the solution with continuous stirring at room temperature at 370 rpm for an additional two days to facilitate FEB loading into the PPRs. The final concentration was set at 5% (w/v) for the copolymers (PF127 or Soluplus®) and 7.5% or 15% (w/v) for 2-HPβCD. The dissolved FEB concentration was 0.05 ± 0.002 mg/mL in 7.5% (w/v) 2-HPβCD solution and 0.16 ± 0.02 mg/mL in 15% (w/v) 2-HPβCD solution (Table 1). In the binary system, the FEB concentration was 0.12 ± 0.01 mg/mL in mixed PF127/2-HPβCD PPRs and 0.24 ± 0.02 mg/mL in mixed Soluplus®/2-HPβCD PPRs. In tertiary systems, the concentration was 0.28 ± 0.05 mg/mL in PF127/Soluplus®/2-HPβCD PPRs with 7.5% (w/v) of 2-HPβCD and 0.31 ± 0.03 mg/mL in PF127/Soluplus®/2-HPβCD PPRs with 15% (w/v) of 2-HPβCD (Table 1). Dispersions containing only the copolymers and drug at the same final concentration were also prepared for comparison. The formulations were filtered through 0.22 μm cellulose filters before DLS and HPLC analysis. The experiment was repeated three times, and the results presented as the mean ± SD.

2.5. Characterization of fenofibrate-loaded poly(pseudo)rotaxanes

2.5.1. X-ray powder diffraction characterization

X-ray powder diffraction (XRD) patterns were obtained using a Bruker D8 Advance X-ray diffractometer in Bragg-Brentano set up. Approximately 10 mg of each sample was used for the analysis. Samples were irradiated with monochromatized CuKα radiation (λ = 1.5406 Å) at a scan rate of 1° per minute over the 2θ range of 2° to 65°. The XRD measurements were performed at room temperature (25 °C).

2.5.2. Proton nuclear magnetic resonance spectroscopy (^{1}H NMR)

^{1}H NMR (Joel ECX) was used to elucidate the molecular structure of the samples. The ^{1}H NMR spectra were recorded on a high-field NMR spectrometer at a proton frequency of 399.79 MHz. Before analysis, the freeze-dried samples (7.14 mM 2-HPβCD, 0.79 mM PF127, 0.085 mM Soluplus® and 10 mg of F1 and F3 formulations) was completely dissolved in D_2O (1 mL). The NMR measurements were carried out at a controlled temperature of 25 °C, and the free induction decay (FID) signal was collected by a standard 90° pulse sequence before analysing through Fourier transformation process to obtain the ^{1}H NMR spectrum. The spectral acquisition parameters included 64 scans and a relaxation delay of 16 s. ^{1}H NMR of 2-HPβCD (D_2O, δ ppm): 3.38 (H-4, —O—C**H**(CH)—CH—), 3.48 (H-2, —CH—C**H**(OH)—), 3.75 (H-5, CH— (CH_2)C**H**—O—), 3.77 (H-6, —C**H**(OH)—CH—), 3.84 (H-3, (HO)C**H**(CH)—CH—) and 4.97 (H-1, —O—C**H**(OH) —). ^{1}H NMR of PF127 (D_2O, δ ppm): 1.06 (—C**H$_3$**—C(=O)—C— protons in PPO blocks), 3.45 and 3.46 (—O—C**H**(CH_3) —C— and —O— (CH_3)CH—C**H$_2$**—O- units of PPO block), 3.60 (—O—C**H$_2$**—CH_2—O— units of PEO blocks). ^{1}H NMR of Soluplus® (D_2O, δ ppm): 1.66 (—C**H$_2$**—C**H$_2$**— unit of poly(vinyl-caprolactam) (PNVCL), 1.97 (—C**H$_3$**—C(=O) —O— unit in polyvinyl acetate (PVA)), 2.41 (—C**H$_2$**—C(=O)—N unit of PNVCL), 3.60 (—O—C**H$_2$**— unit of PEG blocks).

2.5.3. Particle size analysis of fenofibrate formulations

Z-Average Hydrodynamic Diameter (Z-Avg size), polydispersity index (PDI), and zeta potential (ZP) values of the FEB formulations were measured without dilution using a Malvern Zetazier Ultra-Red analyzer (Malvern Panalytical, UK) (Stetefeld et al., 2016; Pecora, 2000). FEB solution with a sample volume of 1 mL was transferred to a 10 mm square polystyrene disposable cuvette (DTS0012), and the instrument temperature was set at 25 °C with light scattered by the sample at a backscattering angle of 173°. For ZP measurement, the same sample at 1 mL was injected into a polycarbonate disposable folding capillary cell with a gold-plated beryllium-copper electrode (DTS1070), rinsed with MilliQ water and sample dispersion before filling. The refractive index of the micelles and water were set at 1.46 and 1.33, respectively, and the ZP measurement samples were equilibrated in the instrument chamber for 120 s at 25 °C. All results presented as the mean ± SD with triplicate measurement for each to ensure reproducibility (n = 3).

2.5.4. Stability study of fenofibrate formulations

The FEB-loaded micelles and mixed micelle solutions, as prepared in Section 2.3 and 2.4, were stored in glass vials at 25 °C for 7 days. The samples were collected and analyzed by DLS to assess changes in the particle sizes and PDI values. Drug retention percentage in the FEB formulations at Day 7 was also determined using HPLC (n = 3).

2.5.5. Viscosity study of fenofibrate formulations

The viscosity of the FEB formulation solutions was measured using the AR-G2 magnetic bearing rheometer (TA Instrument Ltd, US)

equipped with cone and plate geometry (Peltier plate steel). Before the measurement, the viscometer was calibrated using ASTM oil standard, a standard viscosity reference fluid, with the inertia set at 9.40 μN.m.s^2. The following parameters were selected for the geometry setting: diameter (40 mm), gap (500 μm), loading gap (30000 μm), and trim gap offset (500 μm). Then, 1 mL sample volume of the FEB solution was loaded onto the lower plate of the rheometer, and the upper plate was lowered to the desired gap distance. The temperature of the sample was controlled using the Peltier system to maintain a constant temperature throughout the measurement at 25 °C. The viscosity data obtained from the slope between stress and strain rate were recorded and analyzed using TRIOS software. Each measurement was performed in triplicate (n = 3).

2.6. Cytotoxicity study of fenofibrate formulations

Immortalized human corneal epithelial (IM-HCE) cells were cultured in ocular epithelia cell medium supplemented with 5% (v/v) FBS, 1% (v/v) epithelial cell growth supplement (EpiCGS) solution, and 1% (v/v) penicillin/streptomycin solution at 37 °C in a humidified atmosphere with 5 % CO_2. IM-HCE cells were seeded in 96-well plates at a density of 5000 cells/well for 24 h. After that, the cell medium was removed and treated with sterilized (30 min under UV light) free FEB, FEB-loaded single and mixed micelles, FEB-loaded PPRs, and the blank PPR formulation (as the control) at the highest ratio of polymer components without drug at various concentrations ranging from 0.5 to 70 μg/mL for 24 h (Tapia-Guerrero et al., 2020; Bernal-Chávez et al., 2021). Cytotoxicity was assessed using an acid phosphatase colorimetric (APA) assay. After the 24 h treatment with the listed test formulations, the wells were washed three times with 0.01 PBS (pH 7.4), followed by the addition of the para-nitro-phenylphosphate substrate (100 μL) and incubated for 2 h (37 °C, 5% CO_2). Then, 20 μL of 1 M NaOH, a stop solution, was added to each well, and the analysis was performed by fluorescence intensity measurement at an absorbance wavelength of 405 nm using a BioTek Epoch®microplate reader (Agilent Technologies, Dublin, Ireland). The measurement for each sample was repeated in triplicate (n = 3).

2.7. Ex vivo corneal and scleral permeability study of fenofibrate formulations

An *ex vivo* permeation study was carried out on porcine cornea and sclera, according to the method previously described by Pescina *et al* (Pescina et al., 2019; Pescina et al., 2015). Fresh porcine eyes, from Large White and Landrace breed pigs of mixed male and female sex and approximately 22 weeks of age, received from a local abattoir (Dawn meats, Grannagh Business Park, Waterford, Ireland) were obtained immediately after slaughter and stored in a container covered with ice so as to maintain integrity. After being transported to the laboratory, the eyeballs were rinsed with 0.9% NaCl solution to remove blood and other contaminants before immersing in PBS at 4 °C. The corneal and the scleral tissues were used within 6 h after extraction from the eyeballs in the laboratory, and permeation studies were conducted using a Franz diffusion cell with the permeation area of 1.13 cm^2, in line with the method employed in previous studies (Resende et al., 2017; Barbalho et al., 2023; da Silva Gonçalves et al., 2024). Due to the design of the Franz diffusion cells, it was not possible to preserve the curvature of the tissues, as was outlined in the study of Vivero-Lopez *et al.*, where the curvature of the tissue was not maintained during *ex vivo* permeation experiments (Vivero-Lopez et al., 2022). While some studies, such as Pescina *et al.*, used a specific permeation area to minimize tissue distortion from its natural curvature, our study employed a larger permeation area (1.13 cm^2) to maximize drug permeation into the receptor chamber for improved drug quantification by HPLC (Pescina et al., 2019; Pescina et al., 2015). This selection ensured proper alignment of the tissue and solution in both the donor and receptor chambers for *ex vivo* corneal and scleral permeation studies, in line with established methods (Pescina et al., 2019; Pescina et al., 2015; Vivero-Lopez et al., 2022). The cornea and sclera were excised and mounted on the receptor compartment of the diffusion cell, with the endothelium side (the corneal experiment) and the stromal side (the sclera experiment) facing the receptor chamber. After that, the donor compartment of the Franz diffusion cell was applied and clamped. The receptor chamber was filled with PBS solution containing 1% (v/v) Tween 80 (4 mL), which was degassed under a sonicator for 15 mins before adding to the receptor chamber, and the donor chamber was filled with 200 μL of PBS. A 1% (v/v) Tween 80 in PBS solution was selected based on its used in previous studies to enhance drug solubility without causing toxicity to cells (Sitovs and Mohylyuk, 2024; Tao et al., 2013; Chen et al., 2017). In this study, the solubility of FEB in 1% (v/v) Tween 80 was 132 ± 4 μg/mL. The Franz cell was thereafter incubated for 30 min at 37 °C in the incubator before replacing the PBS solution in the donor compartment with the FEB formulation samples (17 μg/mL) and the control groups, i.e. free FEB suspension (17 μg/mL) and PBS solution at the same volume (200 μL), followed by covering the donor chamber with parafilm and aluminium foil. The experiment was performed in an incubator (120 rpm, 37 °C). At predetermined time points, 200 μL of the medium in the receptor chamber was removed using a 1 mL syringe, and the withdrawn samples were replaced with fresh receptor solutions to maintain sink conditions throughout the study. After 6 h, the remaining FEB formulation was removed from the donor chamber, the tissues were washed with 2 mL MilliQ water, dried with filter paper, cut into small pieces and immersed into 2 mL ACN in 20 mL vials. The drug retained in the tissue was extracted by sonication for 5 min. The concentration of the extracted drug solutions was filtered with 0.22 μm cellulose filters before HPLC analysis. Similarly, the concentration of FEB in the withdrawn samples was analyzed using HPLC by diluting with 800 μL of ACN (Pescina et al., 2019). Experiments were repeated nine times (n = 9 eyes). The formulations listed in Table 1 represented the original, undiluted formulation, whereas the formulations were diluted to achieve a FEB concentration of 17 μg/mL in this *ex vivo* permeation study as follows: F1 (13x), F3 (18x), F4 (7x), F5 (14x), C1 (8x), and C4 (9x) (Table S1). Although the formulations were diluted, the particle sizes and the stability remained stable with the properties reported in Table 1 (Fig. S1). The C_s value as shown in Table 2 represents the total retention concentration of drug extracted from the tissue analysed by HPLC (μg/mL). In contrast, the data presented in Fig. 7I and 7II (Y-axis, μg/mg tissue) corresponds to the total extracted drug amount (μg) divided by tissue weight (mg).

2.8. Analytical method validation

A calibration curve was conducted using HPLC analysis with the FEB concentration ranged from 1 to 10 μg/mL. The linear regression equation was Y = 62.34x − 0.0889 with a correlation coefficient (R^2) of 0.9999 (Fig. S2). The limit of detection (LOD) and limit of quantification (LOQ) were 0.03 and 0.09 μg/mL, respectively. To confirm the sensitivity, accuracy and precision of the HPLC method, the lowest detected concentration of permeated FEB drug in the *ex vivo* permeation study was 0.11 μg/mL, which was above the LOQ. This confirmed that this calibration curve could reliably quantify FEB drug permeation across the tissue. The precision of the *ex vivo* permeation study was assessed by evaluating intra-day and inter-day variability of standard FEB in ACN at 10 μg/mL by using HPLC. The intra-day %RSD ranged from 0.07% to 1.37%, while the inter-day %RSD ranged from 1.14% to 3.78%. These values were within the acceptable limits (<15%) according to EMA guidelines for the validation of bioanalytical methods, supporting the robustness of the HPLC method (European Medicines Agency, 2011). The extraction procedures were conducted, and the percentage of drug extracted from the tissue was calculated by dividing the amount of drug extracted from the tissue by the amount of drug initially added, then multiplying by 100. Similarly, drug quantification in other

compartments (the remaining injected solution on the tissue, the amount of drug in 2 mL MilliQ water from the washing step, the solution adhering to the donor cap, and the amount of FEB drug that permeated into the receiving chamber) was performed by calculating the ratio of the extracted amount to the initially added amount of drug, expressed as a percentage. In the *ex vivo* permeation study, the total drug extracted ranged from 32% to 72% for corneal tissue, and 58% to 98% for scleral tissue (Table S2).

2.9. Mathematical model description

The apparent permeability coefficient (P_{app}) is a parameter that provides information about the ability of the drug to penetrate the ocular tissue and is calculated using the following equation:

$$P_{app} = J/C_D \quad (1)$$

Where

J = the flux across full-thickness of the tissue (μg/cm^{2}min) calculated as the slope of the regression line at the steady state of the drug concentration–time profile
C_D = the initial concentration of the drug in the donor chamber at the start (μg/mL)

2.10. Liquid chromatograph mass spectrometry of fenofibrate formulations

Samples collected from the donor chamber at the start of the *ex vivo* permeation study, as per Section 2.7, were prepared by diluting with 50% (v/v) ACN aqueous solution, using 200 μL of the sample mixed with 800 μL of the solution. Whereas samples withdrawn from the receiving chamber were diluted directly with ACN using the same 1:4 sample to solvent ratio. The mixture was then filtered through a 0.45 μm filter for analysis. A HPLC equipped with a EclipsePlus C18 RRHD column (50 x 2.1 mm, 1.8 μm) was used for separating the analytes and detection was at wavelengths of 200, 254 and 285 nm. The mobile phase consisted of a gradient solution between solvent A (water) and solvent B (ACN) at 0.5 mL/min of a flow rate. A gradient method was used that started with running the mobile phase with A:B ratios of 50:50% (v/v) for 15 min before adjusting the mobile phase ratios between A and B to 25:75% (v/v) and held for 5 min. The liquid chromatography/mass spectrometer (LC/MS) was performed using an Agilent 6545 Q-TOF equipped with an dual AJS electrospray ionization (ESI) source (Agilent Cross lab 6545 Q-TOF, Ireland). The instrument setup was operated in positive ion polarity mode with a scan range of m/z 50–1700. MassHunter qualitative analysis 10.0 software was used for data analysis and the quantification of the analytes in the collected FEB formulation samples was calculated based on the calibration curves of the FEB drug and CD on its owns. FEB was quantified using a calibration curve with demonstrated linearity in the range of 0.1–10 μg/mL (LOD = 1.34 μg/mL, LOQ = 4.08 μg/mL) with RSD% and RE% of 0.48 and 1.45, respectively, across all concentration levels. The calibration curve of CD (0.5–50 μg/mL) illustrated LOD of 2.47 μg/mL and LOQ of 7.51 μg/mL, with RSD% of 1.66 and RE % of 15.

2.11. Statistical analysis

Statistical significance was assessed using One-way ANOVA followed by Dunnett's multiple comparison tests for the solubility of FEB formulations in different PF127:Soluplus®:2-HPβCD ratios, cytotoxicity and *ex vivo* permeation studies. Additionally, the FEB solubility at each polymer concentration of PF127 and Soluplus® was analyzed using the independent sample *t*-test. Statistical significance was considered at $p \leq 0.05$. Data analysis was performed using GraphPad Prism software version 10.1.1 (Boston, MA, USA).

3. Results and discussion

3.1. Fenofibrate solubility in different copolymers

This study focused on improving the solubility, and by extension the bioavailability, of FEB using the copolymers PF127 and Soluplus®. As a starting point, the solubility of FEB in PBS solution (pH 7.4) with different copolymers was examined (Fig. 1). The solubility of FEB in PBS solution (0% block copolymer) was 0.34 ± 0.0011 μg/mL, corresponding to previous studies (Lynnerup et al., 2023; Abedin Zadeh et al., 2023). Increasing the concentration of both copolymers in the PBS medium resulted in increased FEB solubility (Fig. 1), with the solubility of FEB in the presence of PF127 higher than with Soluplus® at concentrations > 3% (w/v). The reason may be attributed to the fact that PF127 molecules (hydrophilic-lipophilic balance, HLB = 22) have more hydrophilic parts as compared to Soluplus® (HLB = 16) (Varela-Garcia et al., 2018). Similar investigations were carried out by Lorenzo-Veiga *et al* (Lorenzo-Veiga et al., 2019). They observed an increase in the solubility of natamycin for both copolymers at concentrations equal to or above 1% (w/v). In contrast, the increase was significantly greater for Soluplus® dispersions (~140 μg/mL at 5% (w/v) Soluplus® concentration in 0.9% NaCl solution) due to the lower hydrophobicity of Soluplus® compared to Pluronic® P103 (PF103) (HLB = 9) (Varela-Garcia et al., 2018). Hence, this present study demonstrated that PF127, a triblock copolymers with higher hydrophilic segments, could improve its ability to solubilize hydrophobic drugs like FEB more effectively than Soluplus®.

3.2. Preparation of poly(pseudo)rotaxane formulations

A study to find a suitable ratio between Soluplus® and PF127 to form PPRs was conducted to determine the optimal polymer composition, with the results shown in Fig. 2. The findings illustrated that the 1:1 ratio of PF127 to Soluplus®, was the optimum condition, resulting in the highest FEB solubility reaching around 230 μg/mL, which was in agreement with previous findings showing that the mixed micelles could enhance the drug loading compared to the single micelles (Lorenzo-Veiga et al., 2019; Sun et al., 2020). While, either increasing or decreasing the ratio between PF127 and Soluplus® caused a slight decrease in the solubility of FEB (Fig. 2).

Therefore, a combination of the previous finding and the present study as shown in Fig. 2, led to select 5% (w/v) PF127, 5% (w/v) Soluplus®, and the binary systems with 1:1 ratio of PF127 and Soluplus® in PBS solution (pH 7.4) for the formation of PPRs with 2-HPβCD. The 2-

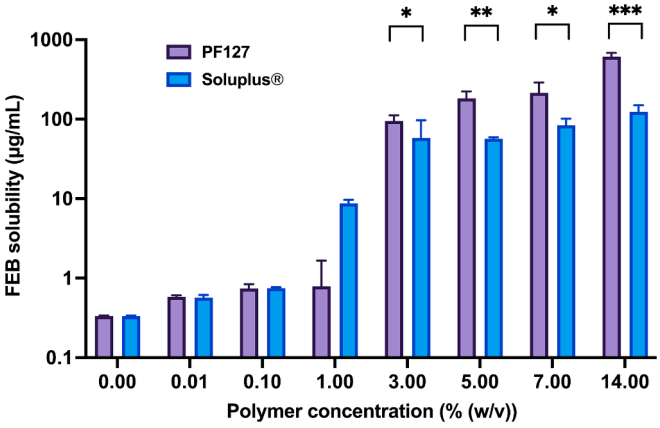

Fig. 1. Solubility of FEB in PF127 and Soluplus® dispersions (0–14% (w/v)) prepared in PBS (pH 7.4) at 25 °C. Data presented as the mean ± SD (n = 3). Statistical significance was analyzed by the independent sample *t*-test (*$p < 0.05$, **$p < 0.01$ and ***$p < 0.001$ compared between the mean values of FEB solubility at each polymer concentration of PF127 and Soluplus®).

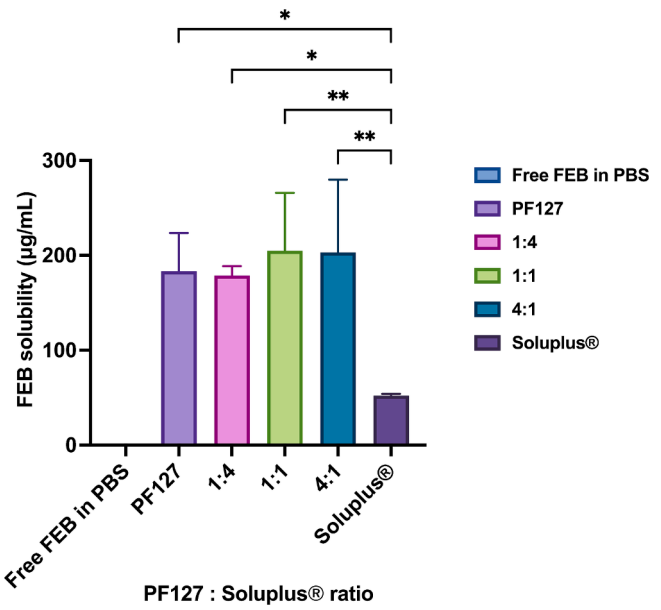

Fig. 2. Apparent solubility of FEB in micelle dispersions of 5% (w/v) of Soluplus® and 5% (w/v) of PF127 and their mixtures (total 10% (w/v)) prepared at various ratios in PBS (pH 7.4) (n = 3). Statistical significance was analyzed by the One-way ANOVA followed by Dunnet's multiple comparisons (*$p < 0.05$ and **$p < 0.01$ compared to the mean values of the average FEB solubility in Soluplus®).

HPβCD was used for this investigation at two different concentrations: 7.5% and 15% (w/v) according to a literature report of safety concerns to prevent testing of a higher concentration of 2-HPβCD above 15% (w/v) (Agency, 2014). Table 1 illustrated the polymer component, the solubility of FEB in each prepared formulation, and the particle size distribution.

The results showed that single micelles, mixed micelles, and PPRs of FEB with PF127, Soluplus®, and 2-HPβCD were successfully formed, and achieved small particle sizes (<100 nm). On the other hand, the 2-HPβCD copolymer at the two concentrations used as a control had particle size distribution ranging from 3 nm to 33 nm. The particle sizes of the single PF127 and Soluplus® micelles were found to be around 55 nm and 61 nm, respectively. Additionally, the mixed PF127/Soluplus® micelles and the PPR formulations exhibited particle sizes ranging from 58 to 67 nm. This can be attributed to the complexation and assembly behaviour of the polymers and 2-HPβCD. In other words, when PF127 or Soluplus® polymers were used alone, they formed smaller micelles owing to self-assembly driven by their amphiphilic nature. However, when mixed with CDs to form PPRs, the inclusion of complexation and host–guest interactions between the polymers and CDs lead to the formation of larger structures, namely mixed micelles and PPRs, due to the increased complexity of the assembly resulting from the diverse host–guest interaction between the polymers and the CDs (Krawczyk-Santos et al., 2022; Öztürk et al., 2022).

Moreover, the increase in apparent solubility of FEB was evident in the PF127/Soluplus® mixed micelles at concentrations of 5% (w/v) (0.23 mg/mL, F1, Table 1). The addition of 2-HPβCD (either 7.5% or 15% (w/v)) resulted in a significant increase in FEB solubility up to 0.31 mg/mL compared to the drug-loaded mixed micelles ($p < 0.05$) (F2 and F3, Table 1), supporting the synergistic effect of 2-HPβCD for enhancing drug solubility. Thus, the present study revealed that the solubility of FEB was enhanced in single and mixed micelles as well as PPRs, in comparison to the free drug. This improvement could have been a result of the FEB drug being encapsulated within these nanocarrier structures by hydrophilic polymer complexation and inclusion complex formation with the CD.

The stability of the FEB formulations was assessed at room temperature for 7 days, and no significant difference in the particle sizes and drug content change at Day 7 compared to Day 0 (after preparation) (Table S3). Furthermore, this present study demonstrated that an increase in formulation components corresponded to an increase in the viscosity of the FEB formulations, ranging from 2.8-6.9 mPa.S (F1-F5, Table 1). Applying this to the OcDD applications, the viscosity of the administered drops is a vital factor that may impact the rate of drainage (Phan et al., 2023). A low viscosity, measured in the range of 1–12 mPa.s, was often preferred for eye drops in OcDD to ensure that they were well-tolerated and could quickly disperse across the eye without causing discomfort or blurring of vision. In accordance with the review by Singh *et al.*, the viscosity between 2 and 3 mPa.s. was appropriate for ocular preparation. (Singh et al., 2020) Similar to the work of Arif *et al.* in evaluating the viscosity of 18 artificial tears, they demonstrated that the mean viscosity for all 18 artificial tears was 12 ± 10 mPa.s (Arif et al., 2020). Considering this, the viscosity of the FEB formulations in the present study were in the range or below the recommended limits for ocular preparation. This suggested that the prepared FEB formulations were suitable to use as eye drops, offering efficient drug delivery with patient comfort.

Overall, the studies on particle size and FEB solubility supported the idea that Soluplus® and PF127 could solubilize FEB in their micelles and interact with 2-HPβCD to form small particle size PPRs, which could act as potential OcDD nanocarriers by enhancing ocular penetration of FEB, a poorly water-soluble drug, as highlighted in the review by Jansook *et al* (Jansook and Loftsson, 2022). Also, this study provided valuable insights into the behaviour of the drug within the polymer systems, laying the groundwork for the subsequent confirmation of PPR formation in the next section.

3.3. *Confirmation of poly(pseudo)rotaxane formations*

The calculation of the drug/CD molar ratio is a crucial factor in forming drug/CD complexes. It evaluates the stoichiometry of the complexation and the efficacy of the drug encapsulation (Saokham et al., 2018). Also, it is essential in optimizing the complexation process and

Table 1
Characteristics of CD-micelle combined systems prepared in PBS (pH 7.4), including Z-Avg size (nm), PDI, ZP (mV), FEB solubility and viscosity. Numbers represent the mean ± SD (n = 3).

Code	Components (% (w/v))			FEB solubility (mg/mL)	DLS measurement			Viscosity (mPa.S)
	2-HPβCD	PF127	Soluplus®		Z-Avg size (nm)	PDI	ZP (mV)	
F1	–	5	5	0.23 ± 0.08	67 ± 3.4	0.14 ± 0.07	−0.64 ± 1.89	4.7 ± 0.3
F2	7.5	5	5	0.28 ± 0.05	66 ± 0.9	0.02 ± 0.007	−1.06 ± 1.55	5.5 ± 0.5
F3	15	5	5	0.31 ± 0.03	65 ± 1.6	0.02 ± 0.003	−1.16 ± 1.68	6.9 ± 0.2
F4	15	5	–	0.12 ± 0.01	7 ± 1.3	0.45 ± 0.09	−0.91 ± 2.02	3.1 ± 0.9
F5	15	–	5	0.24 ± 0.02	58 ± 0.2	0.01 ± 0.01	−1.79 ± 0.52	2.8 ± 0.6
C1	–	5	–	0.13 ± 0.06	55 ± 7.8	0.49 ± 0.12	−2.09 ± -0.68	1.5 ± 0.6
C2	–	–	5	0.05 ± 0.02	61 ± 0.3	0.03 ± 0.02	−1.95 ± -0.46	1.7 ± 0.4
C3	7.5	–	–	0.05 ± 0.002	33 ± 4.8	0.25 ± 0.07	−2.08 ± -2.38	1.2 ± 0.06
C4	15	–	–	0.16 ± 0.02	3 ± 1	0.24 ± 0.05	−0.31 ± -2.68	1.6 ± 0.1

understanding the behaviour of the resulting inclusion complex for FEB and 2-HPβCD. Hence, to quantify the molar ratio, a phase-solubility diagram was studied to calculate the stoichiometry of the inclusion complex and the stability constant ($K_{1:1}$) of the complexation (Fig. 3). Phase solubility tests confirmed that the CD derivative effectively solubilized FEB in PBS solution (pH 7.4), with linear, A_L-type phase solubility curves according to Higuchi and Connors (Fig. 3) (Khin et al., 2022). The slope of the intersection obtained from the phase solubility profile of FEB in 2-HPβCD was used to calculate the stability constant ($K_{1:1}$), the complexation efficiency (CE), and the drug to CD (D:CD) molar ratio (Saokham et al., 2018). By analyzing the resulting data, the calculation showed that although the $K_{1:1}$ was high (9098), the CE (0.0085) and D:CD (1:118) molar ratios were quite low, which were in agreement with previous research studies (Fenyvesi et al., 2020; Jagdale et al., 2019). Low ratios in CE and D:CD values could be explained by the fact that CDs formed both inclusion and non-inclusion complexes with FEB in aqueous solutions. The non-inclusion could be ascribed to that free CD molecules or free FEB drugs were suspended in the solution, resulting in only a small fraction of both molecules being available to create an inclusion complex (Alopaeus et al., 2021). Thus, the results showed that there was an inclusion complex formation between FEB and 2-HPβCD even though the D:CD value was low.

Nuclear magnetic resonance (NMR) spectroscopy was conducted as qualitative analysis to provide a detailed characterization of the drug/CD inclusion complex and validate the PPR formation, while XRD was used to confirm that the drug had transformed from the crystalline to the amorphous state. In addition, the ^{1}H NMR and XRD were conducted on the undiluted drug-loaded formulations, as detailed in Table 1, to ensure an adequate sample quantity for structural confirmation. Since both NMR and XRD characterizations in these studies were focused on qualitative analysis, the signal consistency of these techniques was unaffected by the sample dilution used in the *ex vivo* permeation study (Table S1). The ^{1}H NMR spectrum of 2-HPβCD showed one peak around 5 ppm and the peaks in the ranges of 3.4-4.0 ppm which were likely corresponded to C–H protons within the glucose rings (Fig. 4(I)) (Yang et al., 2009). Additionally, a weak shift of the H-5 proton of 2-HPβCD, located within the interior of the CD cavity, by 0.002 ppm in the formulation F3 suggested the potential structural modifications or inclusion of FEB drug within the CD cavity (Table S4). The observed shift supported the hypothesis of an inclusion complex forming between FEB and 2-HPβCD. The PF127 polymers showed characteristic peaks belonging to PEO (3.6 ppm) and PPO (1.1 ppm) units (Fig. 4(II)) (Shaikhullina et al., 2020). Similarly, the PEG unit of Soluplus® displayed a peak at 3.6 ppm (Fig. 4(III)). In the mixed micelle formulation (F1), the interaction between PF127 and Soluplus® copolymers caused a slight shift in the poly(vinylcarpolactam) (PNVCL) (0.015 and 0.008 ppm) and polyvinylacetate (PVA) (0.016 ppm) unit peaks of Soluplus® (Fig. 4(IV) and Table S4). Comparable changes were observed in the ^{1}H NMR spectrum of the PPR formulation (F3) containing 2-HPβCD, Soluplus® and PF127, where small proton shifts were observed in Soluplus®: 0.014 ppm and 0.008 ppm for the PNVCL unit and 0.001 ppm for the PVA unit. Moreover, a slight shift in the PEO and PPO protons of PF127 was detected in the F3 formulation (Table S4). These shifts indicated specific supramolecular interactions between the copolymers and the 2-HPβCD cavity. The interaction likely involved the PEO block of PF127 and the PEG unit of Soluplus®, as evidenced by changes in the chemical shifts in the NMR spectra of F3 formulation. Hence, the observed shifts in the NMR spectra for the F3 PPR formulation indicated changes in the local electronic environment of the protons caused by specific interactions between the FEB/2-HPβCD complex and the polymers (Simões et al., 2014). In other words, when a polymer interacts with a CD to form a complex, the local electronic environment of the protons in both the polymer and the CD can be affected. The interaction causes a shift in the electrical environment, leading to a change in the resonance frequencies of the protons. This modification was observed by a change in the chemical shifts in the NMR spectra of the F3 PPR sample, which provides supporting evidence for the interactions between the polymers and the CDs. Additionally, these NMR studies confirmed that CD molecules in the aqueous solution interacted with PF127 and/or Soluplus® to form PPRs by threading the linear polymer chains of the copolymer through the hydrophilic outer surface of the cyclic CD molecules, without forming chemical bonds (Simões et al., 2014). Consequently, since CDs did not form inclusion complexes with PF127 and/or Soluplus® micelles, they could only partially encapsulate molecules within their hydrophobic inner cavities (Cheirsilp and Rakmai, 2016). Therefore, in this study, the inclusion complex was observed only between FEB and 2-HPβCD, whereas the cavity of the CDs threading with the polymers to form PPRs was also possible at the exterior surface of the CDs. Moreover, X-ray analysis was conducted for additional understanding of the solid-state structure of the FEB-loaded PPRs with copolymers (Fig. 5). The XRD pattern of the free FEB compound exhibited distinct diffraction peaks indicative of its crystalline nature (Fig. 5(I)). In addition, the XRD pattern of the PF127 polymer showed distinct diffraction peaks at 2θ values of 19.5° and 23.5°, indicating its crystalline structure based on the known crystal structure of PF127 (Fig. 5(II)) (Arukkunakorn et al., 2023). Powdered Soluplus® and 2-HPβCD were amorphous (Fig. 5(III)-(IV)) (Williams et al., 1998; Shamma and Basha, 2013). Also, the physical mixture—a combination of PF127, Soluplus®, 2-HPβCD and free FEB—had diffraction peaks for each component that matched to those of the individual components (Fig. 5(V)). Nevertheless, the XRD pattern of the F3 sample exhibited an amorphous structure, showing a single broad band without a sharp diffraction peak at the 2θ values of 19.0° (Fig. 5(VI)). This indicated that the F3 sample did not show a long-range order or crystalline structure. Overall, the XRD analysis indicates that the FEB forms an amorphous solid dispersion in the free dried PPR formulation.

Taken together, the combined utilization of various analytical techniques, including ^{1}H NMR, XRD and DLS, provided significant evidence that confirmed the successful formation of FEB-loaded PPRs.

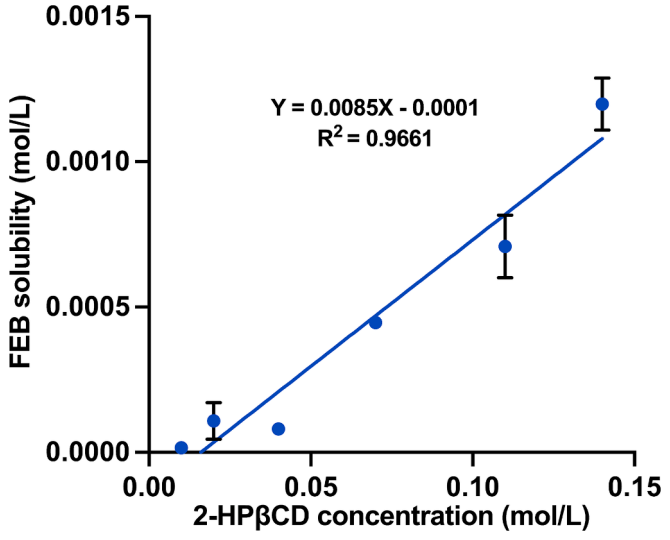

Fig. 3. Phase solubility profile of FEB with 2-HPβCD in PBS solution (pH 7.4) (n = 3).

3.4. Cytotoxicity studies of the fenofibrate-loaded micelles and poly (pseudo)rotaxanes

The study compared the cytotoxicity and biocompatibility of free FEB drug, blank PPR formulations, and FEB-loaded micelles and PPRs on cells, providing insights for potential therapeutic applications and assessing their impact on IM-HCE cells. In the present study, the cell viability analysis was conduct to determine the toxic effects of the free FEB, blank, and FEB formulations on IM-HCE cells using APA assay, as

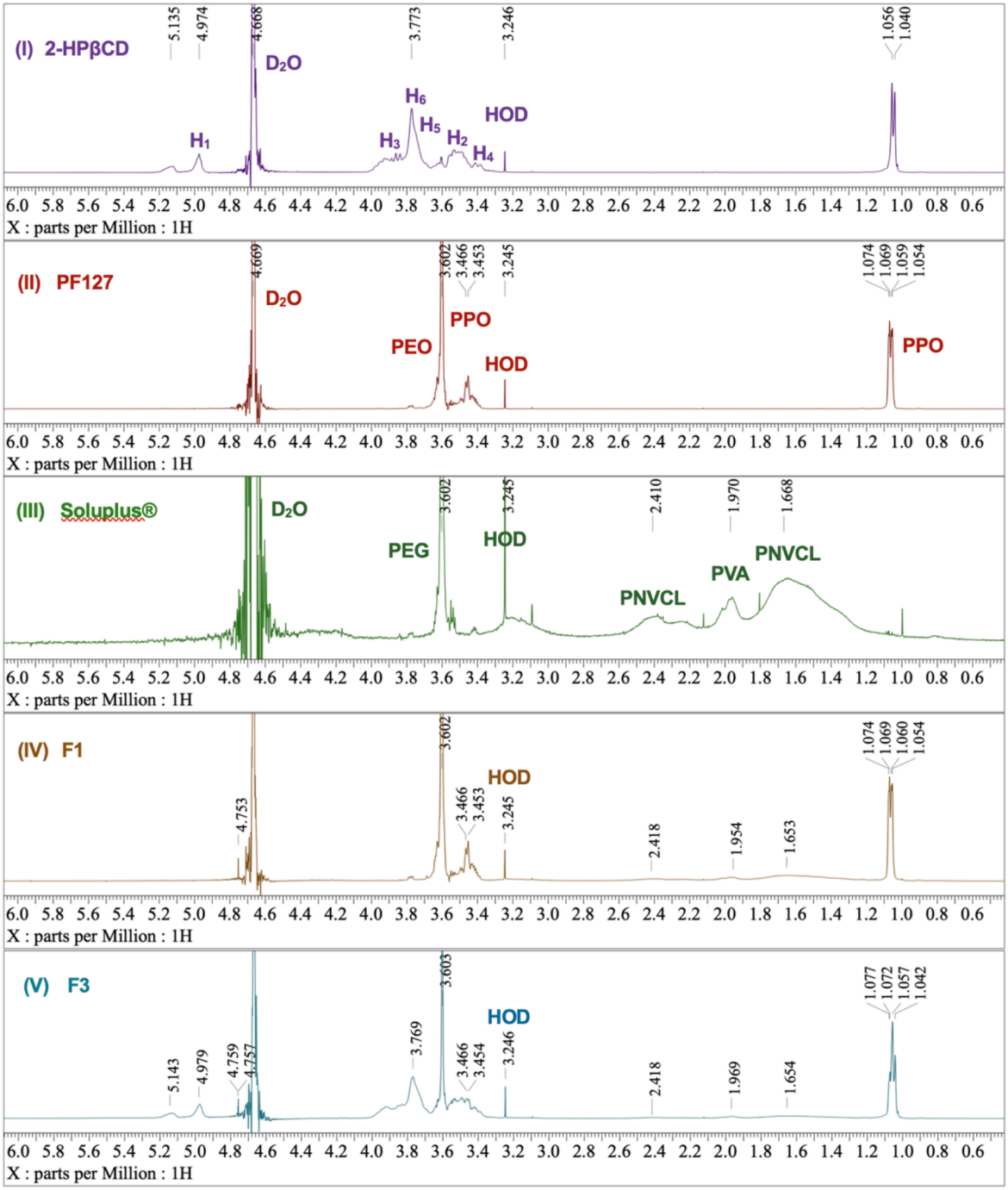

Fig. 4. The ^{1}H NMR spectrum of the raw materials of (I) 7.14 mM 2-HPβCD, (II) 0.79 mM PF127, (III) 0.085 mM Soluplus® (IV) mixed PF127/Soluplus® micelles (F1 from Table 1) and (V) the PPRs (F3 from Table 1) in D_2O (399.79 MHz, T = 25 °C).

per Section 2.6. A graphic summary of the cell viability studies according to IM-HCE cells are shown in Fig. 6. FEB-loaded micelles (C1) and mixed micelles (F1) did not show statistically significant cytotoxic effects on IM-HCE cells while free FEB demonstrated significantly ($p < 0.001$) decreased cell viability at 70 μg/mL, suggesting potential cytotoxic effects of the free FEB drug (Fig. 6(I)). Moreover, cells treated with FEB-loaded single and mixed micelles displayed a significant ($p < 0.05$) decrease in viability at a concentration above 70 μg/mL compared to the medium control (Fig. 6(I)). On the other hand, the cells treated with FEB-loaded PPRs and the control groups of blank PPRs demonstrated a cell viability of over 80% at a concentration below 20 μg/mL (Fig. 6(II)). Our study observed a similar trend in cell viability of FEB formulations reported by Khin *et al.*, which revealed that PVA-stabilized FEB/RMβCD-loaded Eudragit® nanoparticles significantly improved cell viability (>80%) in rabbit cornea cell lines at FEB concentration below 50 μg/mL (Khin et al., 2022).

In conclusion, the results of this cytotoxicity study indicated that the FEB-loaded micelles and mixed micelles were safe at concentrations below 70 μg/mL, and the FEB-loaded PPRs were considered safe at concentration under 20 μg/mL. This supported the inclusion of CDs in the formulation, which has been found to slightly significantly impact the cell viability in our study. By evaluating the effects of the formulation with CDs compared to the formulations without CDs on cell cultures, it was observed that the presence of CDs led to a notable decrease

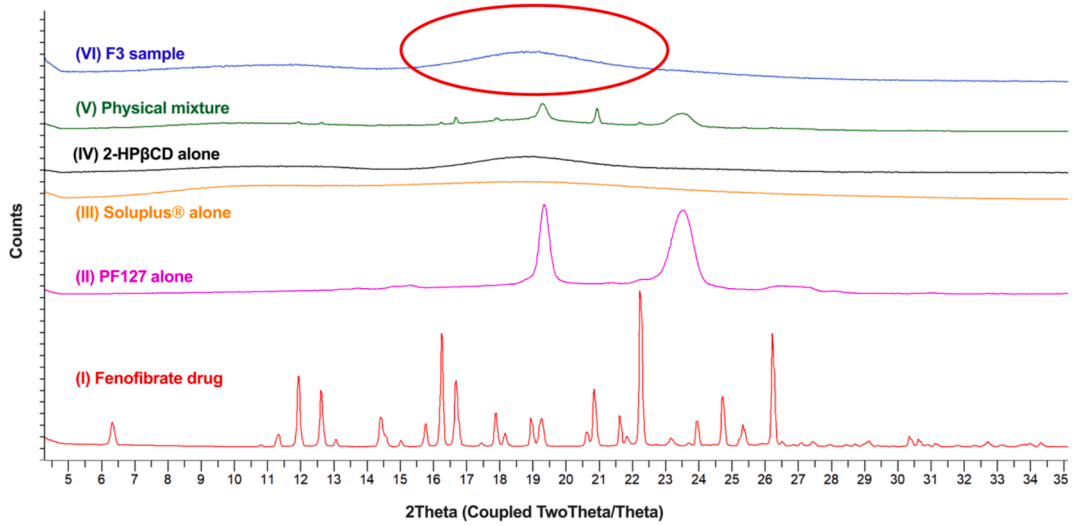

Fig. 5. X-ray diffraction pattern of the individual components: (I) FEB drug, (II) PF127, (III) Soluplus®, (IV) 2-HPβCD, and (V) the physical mixture of FEB, PF127, Soluplus® and 2-HPβCD in the same ratio as the formulation F3, overlaid with (VI) the XRD pattern of formulation F3 (Table 1).

in cell viability. A decline in cell viability can be ascribed to the interactions between CD molecules and the cells, which may impact the integrity of the cell membrane and cellular processes and lead to cell death (Rusznyák et al., 2022). Furthermore, FEB-loaded micelles and PPRs exhibited reduced cytotoxic effects compared to free FEB. These findings highlighted the potential of FEB-loaded micelles/mixed micelles and PPRs as safe and effective delivery systems for the ocular administration of FEB since micelles and PPRs were offered to be biocompatible and could reduce the direct interaction of the FEB drug with the IM-HCE cells, confirmed by the lower cytotoxicity values compared to the free drug at the same concentration in the cell viability study.

Consequently, the FEB-loaded single/mixed micelles and PPRs at a concentration below a toxicity level were selected for further *ex vivo* permeation studies to validate the efficacy of these delivery systems in ocular applications.

3.5. *Ex vivo corneal and scleral permeability study*

To investigate the permeability properties of the FEB formulations and provide insight into potential OcDD applications, an *ex vivo* permeation experiment was carried out on pig cornea and sclera. In this investigation, porcine cornea and sclera were extracted from fresh eyes and mounted in vertical Franz diffusion cells with PBS containing 1% (v/v) Tween 80 as the receptor medium (37 °C). The amount of FEB that permeated through ocular tissues to the receptor chamber was monitored for 6 h with no damage integrity to the cell when using PBS containing 1% (v/v) Tween80 as a receiving medium (Fig. S3), and the results are shown in Fig. 7. Our investigation revealed a permeation of FEB drug into both the corneal and scleral tissues from the single micelles, mixed micelles and PPRs prepared in PBS solution (pH 7.4) (Fig. 7 (I)-(II)). Furthermore, the FEB-loaded PPRs demonstrated measurable penetration through the scleral tissues, while no FEB was detected in the receptor chamber with the corneal tissue for both micelles and PPRs (data not shown). This was within the limit of quantification of the HPLC method, as described in Section 2.8 (LOQ = 0.09 μg/mL and LOD = 0.03 μg/mL for FEB standard calibration ranging from 1-10 μg/mL) (Fig. 7 (III)). The amount of FEB concentration of FEB-loaded PPRs that penetrated across the sclera varied from 0.27 to 4.25 μg/cm^2 (Fig. 7(III)). Besides, the mass spectrometry study confirmed the presence of 2-HPβCD in the receptor chamber of FEB-loaded PPRs across porcine sclera, indicating the potential role of the CD in the transport of the FEB across the scleral tissue (Fig. 7(IV)).

The FEB levels were much higher in the sclera in all prepared formulations (Fig. 7(I)-(II)). The possible reason could be the lower density of tight junctions with relatively large interstitial spaces of the sclera, which could facilitate the retention and distribution of drugs within the sclera due to its permeable nature, as highlighted in the review by Del Amo *et al* (del Amo et al., 2017). In contrast, the compact structure of the cornea composed of multiple layers presents a challenging barrier for drug diffusion compared to the more porous scleral tissue. Other previous studies have observed similar findings in the *ex vivo* permeation of hydrophobic drug-loaded nanocarriers, demonstrating the low transcorneal flux of their formulations (Lorenzo-Veiga et al., 2019; Patil et al., 2018; Ghezzi et al., 2022). Similar results were found in the work by Christensen *et al.* They found that the P_{app} of their cyclic guanosine monophosphate analogue-loaded lipid nanocapsules across the conjunctiva-sclera-choroid-retina was three times higher than that of the full-thickness cornea (666 μm) (Christensen et al., 2023). Thus, these factors collectively contributed to the different levels of drug retention in the cornea and sclera tissues of porcine eyes, emphasizing the importance of understanding the distribution and retention of drugs in specific tissues for the development of efficient OcDD systems.

The study of FEB-loaded PPRs revealed distinct permeability profiles across scleral tissue, thereby enabling the calculation of permeability coefficients for each formulation to quantitatively assess their transport characteristics. The ratio of flux (J) and the concentration of FEB in the donor chamber was used to calculate the P_{app} of FEB over the porcine sclera (Table 2).

The P_{app} value of FEB-loaded PPRs with Soluplus® and 2-HPβCD (F5, 0.047 cm/h) was approximately 3.0 times higher ($p < 0.05$) than the P_{app} values of FEB-loaded PF127/2-HPβCD (F4, 0.014 cm/h) and about 2.5 times higher than those of FEB-loaded PF127/Soluplus®/2-HPβCD (F3, 0.018 cm/h) PPRs (Table 2). This difference may be attributed to the high drug solubility of the FEB-loaded PPRs with Soluplus® and 2-HPβCD (0.24 ± 0.02 mg/mL, Table 1) due to the formation of inclusion complexes with FEB. Furthermore, the increased P_{app} of FEB-loaded Soluplus®/2-HPβCD PPRs could be linked to the effective solubilization and enhanced dissolution of FEB assisted by 2-HPβCD and Soluplus® copolymers, resulting in an improvement of the FEB penetration across the scleral tissue. In contrast, the incorporation system of either PF127 or mixed PF127/Soluplus® micelles with 2-HPβCD in the PPR formulations could disrupt with the permeation of FEB by modifying the structure of the formulation or introducing more complex interactions between the components, thus affecting the P_{app} of FEB. A similar investigation has also been made by Ghezzi *et al.,* revealing that the

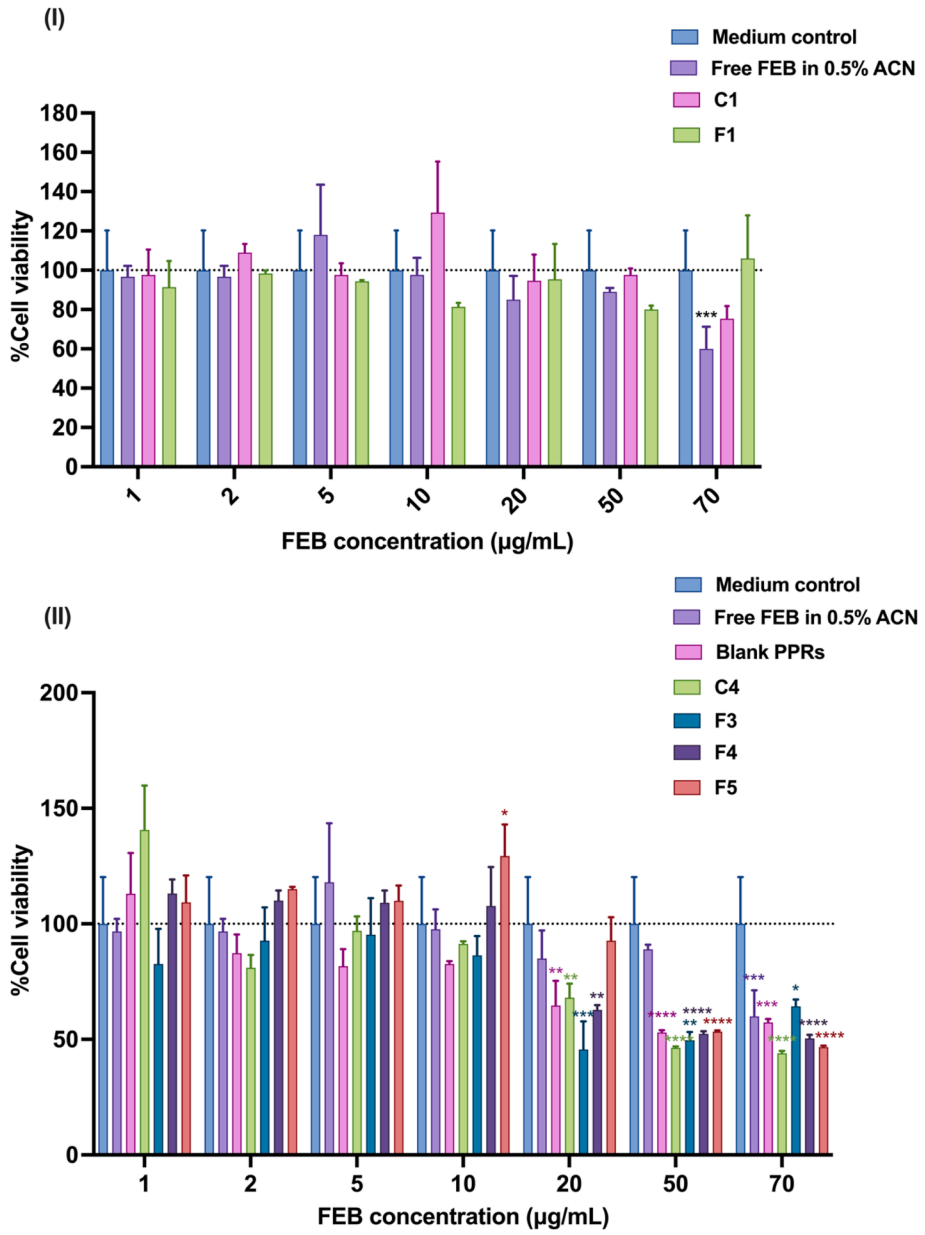

Fig. 6. Assessment of cell viability of IM-HCE cells treated with (I) Free FEB in 0.5% ACN compared to FEB-loaded micelles and mixed micelles (C1 and F1 from Table 1), and (II) Free FEB in 0.5% ACN compared to FEB-loaded PPRs (C4, F3, F4 and F5 from Table 1) and blank PPRs at FEB concentration of 0–70 µg/mL for 24 h. Statistical significance was analyzed by the One-way ANOVA followed by Dunnett's multiple comparisons (*$p < 0.05$, **$p < 0.01$, ***$p < 0.001$ and ****$p < 0.0001$ compared to the mean values of the medium control condition). Data are presented as mean ± SD of three biological replicates (n = 3).

presence of Solutol® HS15 in CsA-loaded TPGS-Solutol® HS15 mixed micelles reduced TPGS metabolism, leading to degradation in contact with ocular tissue in both the porcine cornea and sclera (Ghezzi et al., 2022).

Therefore, the *ex vivo* permeation study of the FEB-loaded micelles and PPRs across corneal and scleral tissues of porcine eyes provided valuable insights into the potential of drug-loaded micelles and PPRs to permeate the ocular barriers, which were critical for effective drug delivery to the eye. More polymer compositions resulted in a more complexed structure of the nanocarriers to deliver drug come across the ocular barriers.

3.6. Mathematical modelling for ex vivo permeation study of the formulations

3.6.1. Development of modelling

The P_{app} is used to calculate the permeability for hydrophobic drugs encapsulated in nanocarriers, even though the nanocarriers are far too big to diffuse across the membrane themselves. The permeability values are then compared across various formulations to determine the preferred formulation to achieve the highest delivery (Pescina et al., 2021). However, the dependency on the permeability of formulations is somewhat misleading because if the same drug is diffusing in both cases of PPRs and micelles, the permeability should be the same, provided that the driving force for the flux is defined as the difference in concentrations of drug in the membrane between the donor and the receiver sides. This assumes that components, such as surfactants, are not acting as permeability enhancers. These components could influence the overall

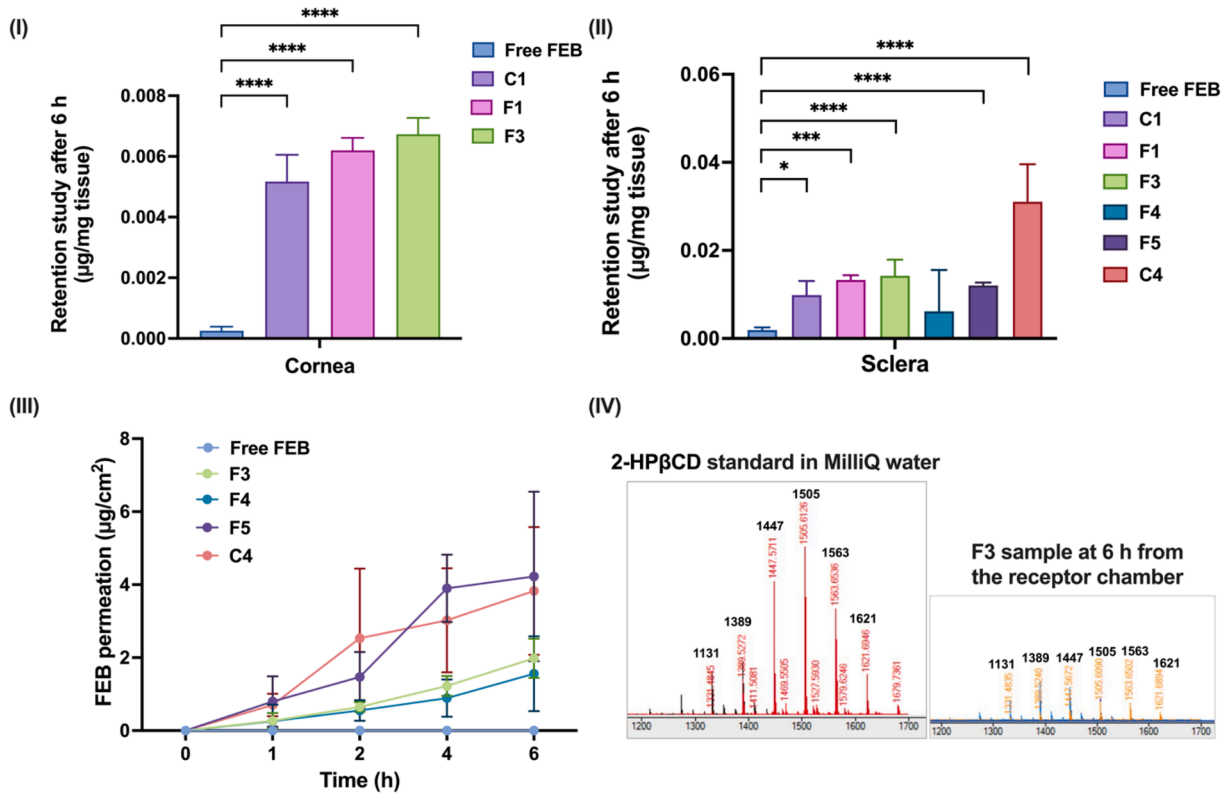

Fig. 7. A graphical representation of drug retention in (I) the cornea and (II) the sclera of the porcine eyes after 6 h of contact with different FEB formulations and the free FEB control. The medium in the receptor chamber is PBS with 1% (v/v) Tween 80. The concentration at the start of the free FEB in the MilliQ water as a control group were 20 ± 9 and 19 ± 1 µg/mL in the cornea and sclera, respectively, (III) permeation profiles of the FEB-loaded PPR formulations across the scleral tissue of the porcine eyes, and (IV) comparing the mass spectrum of a standard of 2-HPβCD in MilliQ water and the composition of the receiving chamber after *ex vivo* permeation study in scleral tissue. Statistical analysis was analyzed by the One-way ANOVA followed by Dunnett's multiple comparisons (*$p < 0.05$, ***$p < 0.001$ and ****$p < 0.0001$ compared to the mean values of the free FEB control group) (n = 9 eyes for each group).

of the formulation permeability by altering the membrane structure or affecting the rate at which the drug permeated from the carriers, resulting in a different in P_{app} values across the formulations (Pescina et al., 2019; Rasoanirina et al., 2020). While using the calculated permeability to choose the preferred formulation is a reasonable approach, a more fundamental understanding of the *ex vivo* transport for nanoformulations will be useful.

Also, it is advantageous to derive this P_{app} calculation from the first principles to understand why the equation may not be directly applicable to nanoformulations and how the equation could be modified to calculate transport parameters for nanoformulations correctly. Understanding the polymer structures could help comprehend how these formulations effectively deliver the drugs to the ocular surface (Fig. 8). This mathematical modelling study was developed to better understand how drug-loaded micelles and PPR formulations penetrated through the tissues.

Based on the *ex vivo* study results, it could be assumed that the micelles were delivering both drug-loaded CDs and the free drug to the corneal or scleral tissues of the porcine eyes (Fig. 7(I)-(II)). The permeation of FEB-loaded PF127/2-HPβCD (F4) and FEB-loaded PF127/Soluplus®/2-HPβCD PPRs (F3) was around two to three-fold lower compared to FEB-loaded 2-HPβCD PPRs (C4) (3.8 µg/cm^2, Fig. 7(III)). Whilst the drug retention of FEB-loaded Soluplus®/2-HPβCD PPRs (F5) was low, the permeability profile of the drug was high in comparison to the FEB-loaded 2-HPβCD PPRs (C4, Fig. 7(II)-(III)). The hypothesis for this model is that the micelle formulations delivered both free drug and drug/CD inclusion complex to the scleral tissue of the porcine eyes and improved the penetration of the drug-loaded CDs to come across the scleral tissue to the receiver chamber (Fig. 9). The development of this mathematical model was conducted using Fick's law of diffusion to model the drug transport in the membrane (Setapa et al., 2020):

$$\frac{dC_s}{dt} = \frac{D\partial^2 C_s}{\partial x^2} \quad (2)$$

Where.

D = Diffusivity
C_s = the retention concentration of substance in the sclera
x = the section of position being considered
t = time

Table 2
The retention concentration (C_s), trans-scleral steady-state flux (J), and permeability coefficients (P_{app}) recorded for FEB formulated in PPRs results obtained from Fig. 7(III)) after 6 h of *ex vivo* trans-scleral permeation (n = 9). Statistical analysis was analyzed by the One-way ANOVA followed by Dunnett's multiple comparisons (*$p < 0.05$ and **$p < 0.01$ compared to the mean values of F5). Data are presented as mean ± SD of nine replications (n = 9 eyes for each group).

Code	Components, % (w/v)			C_s (µg/mL)	J (µg/cm^{2}h)	P_{app} (cm/h)
	2-HPβCD	PF127	Soluplus®			
F5	15	–	5	3.83 ± 0.26	0.82 ± 0.19	0.047 ± 0.011
F4	15	5	–	2.21 ± 3.37	0.26 ± 0.20**	0.014 ± 0.011*
F3	15	5	5	3.62 ± 0.68	0.31 ± 0.07*	0.018 ± 0.004*
C4	15	–	–	10.1 ± 2.15	0.62 ± 0.16	0.036 ± 0.009

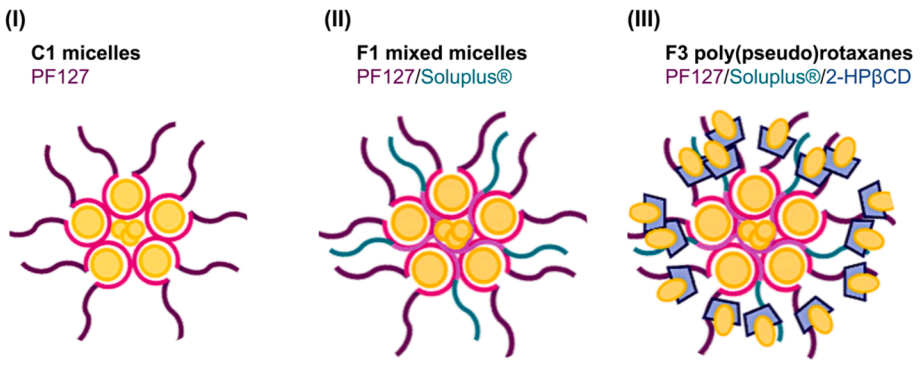

Fig. 8. The schematics of drug-loaded systems: (I) single and (II) mixed micelles formed by self-assembly of the amphiphilic block copolymers, and (III) CD-based PPRs.

Fick's law, according to Eq. (2), describes the rate at which a substance diffuses through a tissue or medium over time. The above differential equation needs to be solved with two boundary conditions and an initial condition (Fig. 9). The boundary conditions typically assume that the concentration of the drug in the donor chamber at position (x) close to the receiver chamber is equal to 0, i,e., at the boundary with the donor chamber is equal to the product of the starting concentration in the donor chamber and the partition coefficient (Fig. 9(I)). Moreover, Eq. (2) assumes that the concentration in the donor chamber remains relatively constant throughout the experiment. The drug concentration at the surface in contact with the receiver chamber is assumed to be zero because the concentration in the receiver chamber is usually very small compared to the drug concentration in the donor chamber. Therefore, the steady state solution to the above differential equation is a linear concentration profile, which refers to a situation where the drug concentration in a particular region remains approximately constant over time even though the drug is continuously diffusing through the medium. The linear profile also implies that the average concentration in the membrane is simply half of the concentration at the boundary with the donor (Fig. 10).

By extension, the concentration at the boundary with the donor is equal to twice the average concentration in the membrane (Fig. 10). The transportation of drug molecules goes from higher to lower concentration across a concentration gradient towards the receiver chamber (Fig. 9(II)). Consequently, the concentration in the receiver chamber can be calculated by equating the rate of accumulation to the rate of flux coming in from the membrane into the chamber (Fig. 9(II)), i.e.,

$$\frac{VdC_r}{dt} = \frac{-D\partial C_s A}{\partial x} \tag{3}$$

Where.

C_r = concentration of a substance in the receiver chamber
t = time
x = the section of position being considered
A = cross-sectional area of the tissue
C_s = the retention concentration of a substance in the sclera

The drug concentration in the sclera was changed so that the concentration of the drug was higher near the donor chamber and lower near the receiving chamber (Fig. 9(I)). However, in this case, due to the straight line of the pseudo-steady state (Fig. 10). Consequently, the measured drug concentration was calculated using the average concentration in the sclera at the boundary according to Eq. (4).

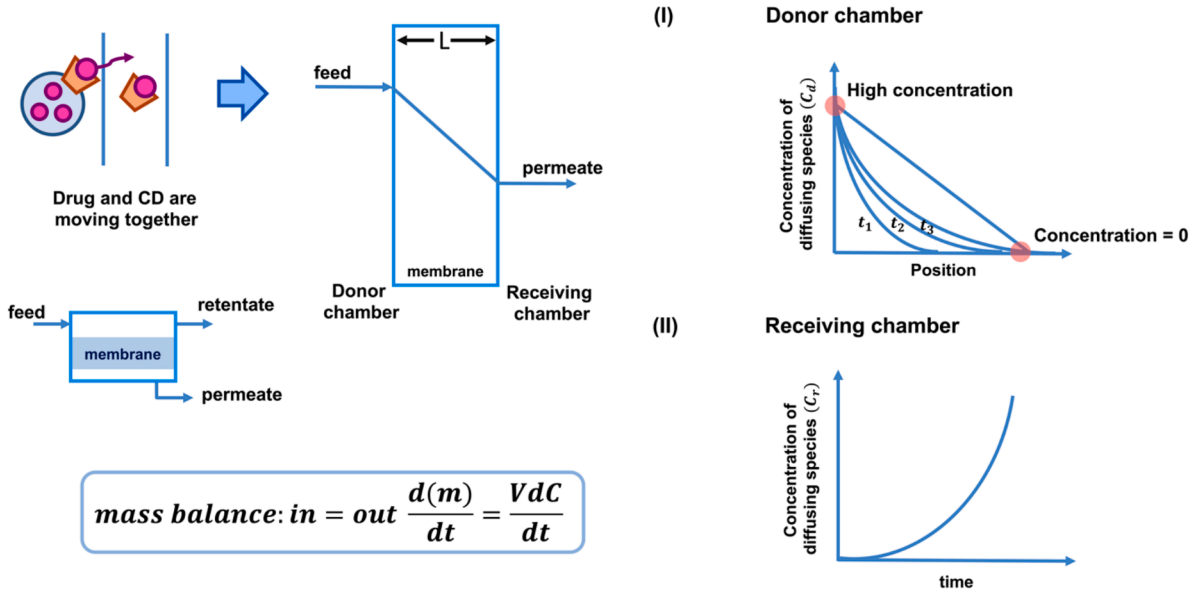

Fig. 9. Schematic representation of the mathematical model design with transport pathway, and the drug permeation profile during the *ex vivo* permeation experiment from (I) the donor chamber to (II) the receiving chamber.

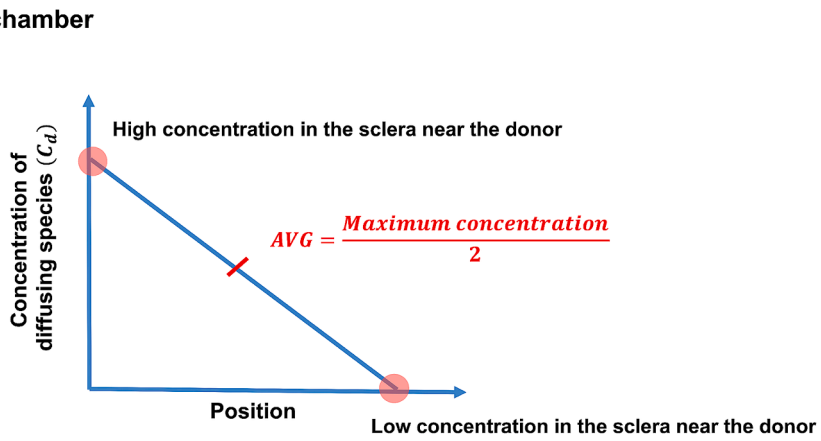

Fig. 10. A plot of the drug permeation profile in the donor chamber at different positions across the scleral tissue of the porcine eyes based on *ex vivo* permeation.

$$< C_s > \ = \frac{KC_d}{2} \tag{4}$$

Where

C_s = concentration of a substance in the sclera
K = the partition coefficient which refers to the ratio of the concentration of a substance in one medium to the concentration in a second phase when the two concentrations are at the equilibrium
C_d = drug concentration in the donor chamber

The effective diffusivity, D_{eff} (cm^2/h), which is a measure of how quickly a molecule diffuses through a medium, while accounting for structural factors such as tortuosity and porosity, was calculated from the flux (J) calculated from the *ex vivo* permeation study. The D_{eff} values represent area per unit time, and by convention is a negative value because of the flow direction higher to lower concentration. Therefore, the equation is further developed from Eqs. (3)–(5).

$$J = -D_{eff}\frac{dC_d}{dX} \tag{5}$$

Where

J = diffusion flux, the net movement of a substance across specified area in a specified time
D_{eff} = effective diffusivity
C_d = concentration of a substance in the donor chamber

Eq. (5) was further developed by including the C_d parameter from Eq. (4), the new equations to obtain D are as follows:

$$J = \frac{D_{eff}\ x\ 2 < C_s >}{L} \tag{6}$$

$$\therefore \boldsymbol{D_{eff}} = \frac{\boldsymbol{JxL}}{2 < \boldsymbol{C_s} >} \tag{7}$$

Where

D_{eff} = effective diffusivity (cm^2/h)
L = thickness of the tissue (cm)
C_s = concentration of the substance in the sclera (μg/cm^3)

Eq. (7) was then applied to the *ex vivo* permeation results to calculate the effective diffusivity (D_{eff}), assuming a scleral thickness (L) of 0.05 cm as per previous reported values of the scleral thickness for porcine eyes. (Olsen et al., 2002).

3.6.2. Model validation

The summary of the *ex vivo* permeation study and the effective diffusivity (D_{eff}) calculation are displayed in Table 3.

The effective diffusivity (D_{eff}) values for the F4 PPR formulations showed no significant ($p > 0.05$) difference compared to F5 PPR formulations (Table 3), indicating similar permeability rates for these formulations. In addition, the D_{eff} of F4 formulation showed a high SD, which was consistent with previous studies reporting high variability of SD in *ex vivo* permeation study (Santana et al., 2023; Cañadas-Enrich et al., 2018). For instance, Santana *et al.* investigated the permeability of various drugs through porcine corneas and observed the high SD in the tissue uptake values of Triamcinolone HA drug (n = 5 corneas) (Santana et al., 2023). Similarly, Canadas-Enrich *et al.* reported high variability in cumulative drug permeation with n = 3 (Cañadas-Enrich et al., 2018). To enhance reproducibility, the number of replicates in our study was increased to n = 9. However, the high SD of the F4 formulation persisted, which could be attributed to intrinsic tissue variability, as commonly observed in *ex vivo* permeation studies. In addition, the D_{eff} for the C4 control formulation (2-HPβCD) and the F3 PPR formulations (PF127/Soluplus®/2-HPβCD) were significantly lower than that of F5 formulation (Soluplus®/2-HPβCD), suggesting that the FEB-loaded PPRs containing single copolymer could enhance drug permeability. Furthermore, based on the $P_{app(t+D)}$ calculation, there was a significant ($p < 0.05$) difference in the $P_{app(t+D)}$ between F3 and C4 with F5 PPRs, which suggested that other factors impacted the drug permeation. This could be explained by the fact that although the $P_{app(t+D)}$ and D_{eff} have separate characteristics, they can be linked together. The permeability ($P_{app(t+D)} = D_{eff}$*K/L) is affected by three factors including the partition coefficient of drug between tissue and the formulation (K), the effective diffusivity (D_{eff}) and the tissue thickness (L), leading to the difference in permeability calculation across the formulations caused by these factors. For example, in this case, F3 PPRs (PF127/Soluplus®/2-HPβCD) consisted of higher polymer compositions than F5 PPRs (Soluplus®/2-HPβCD). A mixture of several composition of polymers might decrease the drug partitions between the tissue and the formulations, resulting in a significant decrease in drug permeability of F3 PPRs (Table 3). Similar results were found in the research work by Lorenzo-Veiga *et al* (Lorenzo-Veiga et al., 2019). They investigated the permeation of natamycin-loaded PF103 micelles, PF103/Soluplus® mixed micelles and PF103/Soluplus®/γ-CD PPRs (~120 nm) across the sclera of bovine eyes. Their study found that the permeability for the drug-loaded PPRs (P_{app} = 0.91 x 10^{-6} cm/s) was smaller than that for the drug-loaded single PF103 (~20 nm) and mixed PF103/Soluplus® (~110 nm) micelles (P_{app} = 1.67 x 10^{-6} and 1.44 x 10^{-6} cm/s, respectively), indicating the enhancement of drug permeation mainly caused by the copolymers. Thus, this mathematical model development indicated that P_{app} was used to estimate drug permeation across tissue which included

Table 3
The retention concentration (C_s), trans-scleral steady-state flux (J), the apparent permeability coefficients (P_{app}), the permeability based on tissue thickness and effective diffusivity ($P_{app(t+D)}$), effective diffusivity (D_{eff}) and drug:CD (D:CD) ratio recorded for FEB formulated in Soluplus® and PF127 micelles, Soluplus®:PF127 mixed micelles, and PPRs in PBS (pH 7.4) solution after 6 h of *ex vivo* trans-scleral permeation. Statistical analysis was analyzed by the One-way ANOVA followed by Dunnett's multiple comparisons (*$p < 0.05$ and **$p < 0.01$ compared to the mean values of F5). Data are presented as mean ± SD of nine replications (n = 9 eyes for each group).

Code	C_s (μg/mL)	J (μg/cm^{2}h)	P_{app} (cm/h)	D_{eff} x 10^3 (cm^2/h)	$P_{app(t+D)}$ (cm/h)	D:CD molar ratio		
						Donor	Receptor	
						Start	1 h	2 h
F3	3.62 ± 0.68	0.31 ± 0.07*	0.018 ± 0.004*	2.16 ± 0.57*	0.009 ± 0.002*	3378: 1	5: 12	4: 1
F4	2.21 ± 3.37	0.26 ± 0.20**	0.014 ± 0.011*	6.11 ± 5.75	0.007 ± 0.006	3292: 1	1: 3	2: 7
F5	3.83 ± 0.26	0.82 ± 0.19	0.047 ± 0.011	5.31 ± 0.94	0.023 ± 0.006	32: 1	1: 5	3: 7
C4	10.1 ± 2.15	0.62 ± 0.16	0.036 ± 0.009	1.63 ± 0.71*	0.018 ± 0.005*	59: 1	1: 1	1: 2
F1	3.80 ± 0.09	–	–	–	–	–	–	–
C1	2.32 ± 0.73	–	–	–	–	–	–	–
Free FEB	1.92 ± 0.59	–	–	–	–	–	–	–

diffusivity and partitioning effects inside the tissue. Whereas, the developed effective diffusivity equation focused primarily on the mechanism of drug diffusion through the tissue. Gaining a comprehension of drug diffusivity aids in optimizing the design formulations, such as altering the polymer compositions, in order to enhance drug diffusivity and provide more effective therapeutic effects.

Furthermore, the D:CD ratio detected for each formulation based on the mass spectrometer characterization was slightly different between the donor and receiver phases, showing that the inclusion complex between D:CD was obtained at various D:CD ratios (Table 3). When formulating drugs using CDs, it was expected to aim for a 1:1 M ratio of the D:CD to maximize complexation efficiency and enhance the solubility and stability of the drug. However, in this case, the addition of excipients such as PF127 and/or Soluplus® copolymers could disturb the 1:1 M ratio between the FEB and 2-HPβCD, obtaining a different optimal ratio for complexation at different times of permeation study. For instance, the surfactants (PF127 and/or Soluplus® copolymers) might have made the layer more permeable, leading to more drug interaction or binding with tissue in the donor phase during the permeation study, which resulted in a lower free drug concentration in the receptor phase. Whereas the CDs with a very small size (~3 nm, Table 1) could penetrate tissue more effectively and deliver the drug in the form of a drug/CD inclusion complex to the receptor chamber, resulting in a relative higher amount of CD and a more detectable amount of D:CD complexes in the receptor phase. Therefore, this study supported the hypothesis that the micelles assisted in the transportation of the drug and D/CD inclusion complex to the tissue. Additionally, CD facilitated the drug to come across the tissue to the receptor chamber via inclusion complex formation. Given the promising drug delivery application, Formulation F5 proved to be the most effective nanocarriers among FEB-loaded PPR developed formulations, showing enhanced drug permeability to across the porcine scleral tissue. Consequently, it is considered a leading nanocarrier for further studies with the potential to be developed into an ophthalmic formulation for topical eye drop administration to treat posterior segment eye diseases.

4. Conclusions

FEB-loaded micelles, mixed micelles and PPR formulations formed by PF127, Soluplus® and 2-HPβCD were successfully prepared. In addition, PPR formulations produced by adding 2-HPβCD to the micelle dispersions significantly increased the water solubility of FEB compared to the only drug-loaded micelles. Multiple analytical techniques, including DLS, ^{1}H NMR, XRD, and DLS confirmed the successful formation of FEB-loaded PPRs. Small size particles ranging between 7 and 67 nm were obtained from the FEB-loaded single micelles (PF127 or Soluplus®), and mixed PF127/Soluplus® micelles as well as PPRs, indicating the potential for improved drug absorption and bioavailability within the eye due to the small size particles (<100 nm). The ^{1}H NMR analysis showed a slight proton shift in the inner wall of 2-HPβCD which supported the formation of an inclusion complexation between the FEB drug and 2-HPβCD. Additionally, proton shifts observed between Soluplus®, PF127 and the exterior cavity of 2-HPβCD in the F3 PPR formulation suggested structural modifications between the copolymers and 2-HPβCD. However, 2D NOESY could further confirm these intermolecular interactions and will be considered in future studies. Furthermore, the XRD pattern of the F3 PPRs exhibited an amorphous halo without a sharp diffraction peak at 2θ values of 19.0°. Therefore, these techniques offered an advantage to better understand the interaction of the copolymers in PPRs and confirmation the formation of PPRs as a nanocarrier. The *ex vivo* permeation studies across the porcine cornea and sclera demonstrated the permeation of FEB single micelles, mixed micelles, and PPRs into the corneal and scleral tissues. Moreover, FEB-loaded PPRs could help to transport the drug across the scleral tissue to the receiver chamber. This *ex vivo* permeation study led to the mathematical model development to clarify the transportation of drug using both micelles and PPR formulations across the tissues. A hypothesis for mathematical model development was the single and mixed micelles delivered both free drug and drug/CD inclusion complex into the scleral tissue, while CDs, in the form of drug/CD inclusion complex, helped to deliver the drug come across the scleral tissue to the receiving chamber. To prove this hypothesis, the modelling was developed and optimized based on Fick's law, and the Fick's law was modified to calculate the effective diffusivity (D_{eff}). This approach included the permeability coefficient (P_{app}) and the retention concentration (C_s) in the equation to better explain how the drug-loaded single/mixed micelles or PPRs transported across the corneal and scleral tissues of the porcine eyes. Also, the effective diffusivity equation was applied to test the validity of the hypothesis by incorporating the *ex vivo* permeation results into the equation. The D_{eff} values for the F4 PPR formulations showed no significant difference compared to F5 PPR formulations, demonstrating similar permeability rates. However, both C4 control and F3 PPR formulations exhibited significantly lower D_{eff} values than F5, highlighting the ability of FEB-loaded PPRs containing single copolymer could effectively enhance drug permeation across the tissue. A similar trend was observed in the P_{app} calculation across the FEB-loaded PPR formulations, where F3 formulation showed lower permeability than F5, further supported this conclusion. In addition, there was a difference in the D:CD ratio in the donor and receiver chambers in all formulations according to the LC/MS characterization, which suggested that the surfactant either PF127 or Soluplus® might affect the permeation of the tissue.

In conclusion, the combination of single and/or mixed micelles with PPRs provided the ability for changing the characteristics of copolymers and CD. For instance, when PF127 and Soluplus® were combined to form the mixed micelles, it resulted in the FEB permeation into the

corneal and scleral tissues of the porcine eyes. Furthermore, FEB could penetrate across the scleral tissues into the receiver chamber when adding CD into the PF127 and/or Soluplus® micelle systems. Thus, the study underlined the crucial role of formulation design in regulating ocular drug permeation and provided valuable insights for creating effective OcDD systems. Additionally, the development of a mathematical model based on Fick's law, which has not been previously reported, demonstrated that this model development aids in clarifying the experimental data, leading to an expanded understanding of the result findings and supporting our hypotheses. This could help to further clarify the role of the study: how CD-based micelles or mixed micelles deliver the drug into the tissues and come across the tissue into the deeper layers. Thus, PPRs of both single and mixed micelles prepared in this research study proved to be an effective nanocarrier for controlled release of the hydrophobic drugs into the deeper layers of the ocular tissues in OcDD application.

CRediT authorship contribution statement

Butsabarat Klahan: Writing – original draft, Software, Methodology, Investigation, Data curation, Conceptualization. **Niall J. O'Reilly:** Writing – review & editing, Supervision, Funding acquisition, Conceptualization. **Hakon Hrafn Sigurdsson:** Writing – review & editing, Supervision, Funding acquisition, Conceptualization. **Anuj Chauhan:** Writing – review & editing, Supervision, Funding acquisition, Conceptualization. **Satu Mering:** Writing – review & editing, Supervision, Funding acquisition. **Laurence Fitzhenry:** Writing – review & editing, Supervision, Project administration, Funding acquisition, Conceptualization.

Declaration of competing interest

The authors declare the following financial interests/personal relationships which may be considered as potential competing interests: Butsabarat Klahan reports financial support was provided by The European Union's Horizon 2020 Research and Innovation Programme under the Marie Sklodowska-Curie Actions (grant agreement number 813440; Ocular Research by Integrated Training and Learning (OTRG)). Laurence Fitzhenry and Niall O'Reilly report a relationship with Ocudel Ltd. that includes: board membership and equity or stocks. The other authors declare that they have no known competing financial interests or personal relationships that could have appeared to influence the work reported in this paper.

Acknowledgements

This project was funded by the European Union's Horizon 2020 Research and Innovation Programme under the Marie Sklodowska-Curie Actions (grant agreement number 813440; Ocular Research by Integrated Training and Learning (ORBITAL). The authors would like to acknowledge the training support provided by Madhuri Dandamudi (Ocular Therapeutics Research Group, Pharmaceutical and Molecular Biotechnology Research Centre, South East Technological University, Ireland) in cell culture study, Marcos Mariano (Pharmaceutical and Molecular Biotechnology Research Centre, South East Technological University, Ireland) in LC/MS analysis, and Abinash Nayak (Pharmaceutical and Molecular Biotechnology Research Centre, South East Technological University, Ireland) in ^{1}H NMR analysis. In addition, the authors would like to thank Dawn Meats, Grannagh Business Park, Waterford, Ireland, for providing pig eyes used in this study.

Appendix A. Supplementary data

Supplementary data to this article can be found online at https://doi.org/10.1016/j.ijpharm.2025.125417.

Data availability

Data will be made available on request.

References

Abedin Zadeh, M., Alany, R.G., Satarian, L., Shavandi, A., Abdullah Almousa, M., Brocchini, S., Khoder, M., 2023. Maillard reaction crosslinked alginate-albumin scaffolds for enhanced fenofibrate delivery to the retina: A promising strategy to treat RPE-related dysfunction. *Pharmaceutics* 15 (5), 1330.

Agency, E.M., 2014. Background review for cyclodextrins used as excipients. EMA London, UK.

Agrahari, V., Mandal, A., Agrahari, V., Trinh, H.M., Joseph, M., Ray, A., Hadji, H., Mitra, R., Pal, D., Mitra, A.K., 2016. A Comprehensive insight on ocular pharmacokinetics. *Drug Deliv. Transl. Res.* 6 (6), 735–754. https://doi.org/10.1007/s13346-016-0339-2.

Alopaeus, J.F., Göbel, A., Breitkreutz, J., Sande, S.A., Tho, I., 2021. Investigation of hydroxypropyl-β-cyclodextrin inclusion complexation of two poorly soluble model drugs and their taste-sensation-effect of electrolytes, freeze-drying and incorporation into oral film formulations. *J. Drug Deliv. Sci. Technol.* 61, 102245.

Alvarez-Rivera, F., Fernández-Villanueva, D., Concheiro, A., Alvarez-Lorenzo, C., 2016. α-Lipoic acid in soluplus® polymeric nanomicelles for ocular treatment of diabetes-associated corneal diseases. *J. Pharm. Sci.* 105 (9), 2855–2863. https://doi.org/10.1016/j.xphs.2016.03.006.

Arif, F.A.C., Hilmi, M.R., Kamal, K.M., Ithnin, M.H., 2020. Evaluation of 18 artificial tears based on viscosity and PH. *Malaysian J. Ophthalmol.* 2 (2), 96–111.

Arukkunakorn, W., Sajomsang, W., Ovatlarnporn, C., 2023. Resveratrol enhance loading capacity and solubility of dimethylcurcumin in pluronic F-127 nanomicelles. Eur. Chem Bull.

Barbalho, G.N., Falcão, M.A., Lopes, J.M.S., Lopes, J.M., Contarato, J.L.A., Gelfuso, G.M., Cunha-Filho, M., Gratieri, T., 2023. Dynamic ex vivo porcine eye model to measure ophthalmic drug penetration under simulated lacrimal flow. *Pharmaceutics* 15 (9), 2325.

Bernal-Chávez, S.A., Del Prado-Audelo, M.L., Caballero-Florán, I.H., Giraldo-Gomez, D. M., Figueroa-Gonzalez, G., Reyes-Hernandez, O.D., González-Del Carmen, M., González-Torres, M., Cortés, H., Leyva-Gómez, G., 2021. Insights into terminal sterilization processes of nanoparticles for biomedical applications. *Molecules* 26 (7). https://doi.org/10.3390/molecules26072068.

Cañadas-Enrich, C., Abrego, G., Alvarado, H.L., Calpena-Campmany, A.C., Boix-Montañes, A., 2018. Pranoprofen quantification in ex vivo corneal and scleral permeation samples: Analytical validation. *J. Pharm. Biomed. Anal.* 160, 109–118.

Cheirsilp, B., Rakmai, J., 2016. Inclusion complex formation of cyclodextrin with its guest and their applications. *Biol Eng Med* 2 (1), 1–6.

Chen, X.R., Besson, V.C., Palmier, B., Garcia, Y., Plotkine, M., Marchand-Leroux, C., 2007. Neurological recovery-promoting, anti-inflammatory, and anti-oxidative effects afforded by fenofibrate, a PPAR alpha agonist, in traumatic brain injury. *J. Neurotrauma* 24 (7), 1119–1131. https://doi.org/10.1089/neu.2006.0216.

Chen, W., Palazzo, A., Hennink, W.E., Kok, R.J., 2017. Effect of particle size on drug loading and release kinetics of gefitinib-loaded PLGA microspheres. *Mol. Pharm.* 14 (2), 459–467.

Christensen, G., Urimi, D., Lorenzo-Soler, L., Schipper, N., Paquet-Durand, F., 2023. Ocular permeability, intraocular biodistribution of lipid nanocapsule formulation intended for retinal drug delivery. *Eur. J. Pharm. Biopharm.* 187, 175–183. https://doi.org/10.1016/j.ejpb.2023.04.012.

da Silva Gonçalves, M., Cabral, L.M., de Sousa, V.P., do Carmo, F.A., 2024. Development of ocular delivery systems for macitentan and ex vivo study of intraocular permeation. *J. Drug Deliv. Sci. Technol.* 100, 106023.

Dehvari, K., Chen, Y., Tsai, Y.-H., Tseng, S.-H., Lin, K.-S., 2016. Superparamagnetic iron oxide nanorod carriers for paclitaxel delivery in the treatment and imaging of colon cancer in mice. *J. Biomed. Nanotechnol.* 12 (9), 1734–1745.

del Amo, E.M., Rimpelä, A.-K., Heikkinen, E., Kari, O.K., Ramsay, E., Lajunen, T., Schmitt, M., Pelkonen, L., Bhattacharya, M., Richardson, D., et al., 2017. Pharmacokinetic aspects of retinal drug delivery. *Prog. Retin. Eye Res.* 57, 134–185. https://doi.org/10.1016/j.preteyeres.2016.12.001.

Elsaid, N., Jackson, T.L., Elsaid, Z., Alqathama, A., Somavarapu, S., 2016. PLGA microparticles entrapping chitosan-based nanoparticles for the ocular delivery of ranibizumab. *Mol. Pharm.* 13 (9), 2923–2940. https://doi.org/10.1021/acs.molpharmaceut.6b00335.

European Medicines Agency, 2011. Guideline on bioanalytical method validation.

Feng, X., Chen, Y., Li, L., Zhang, Y., Zhang, L., Zhang, Z., 2020. Preparation, evaluation and metabolites study in rats of novel amentoflavone-loaded TPGS/Soluplus mixed nanomicelles. *Drug Deliv.* 27 (1), 137–150.

Fenyvesi, F., Nguyen, T.L.P., Haimhoffer, Á., Rusznyák, Á., Vasvári, G., Bácskay, I., Vecsernyés, M., Ignat, S.-R., Dinescu, S., Costache, M., 2020. Cyclodextrin complexation improves the solubility and caco-2 permeability of chrysin. *Materials (Basel).* 13 (16), 3618.

German, C., Chen, Z., Przekwas, A., Walenga, R., Babiskin, A., Zhao, L., Fan, J., Tan, M. L., 2023. Computational model of in vivo corneal pharmacokinetics and pharmacodynamics of topically administered ophthalmic drug products. *Pharm. Res.* 40 (4), 961–975. https://doi.org/10.1007/s11095-023-03480-6.

Ghezzi, M., Ferraboschi, I., Delledonne, A., Pescina, S., Padula, C., Santi, P., Sissa, C., Terenziani, F., Nicoli, S., 2022. Cyclosporine-loaded micelles for ocular delivery: investigating the penetration mechanisms. *J. Control. Release* 349, 744–755. https://doi.org/10.1016/j.jconrel.2022.07.019.

Hanaguri, J., Nagai, N., Yokota, H., Kushiyama, A., Watanabe, M., Yamagami, S., Nagaoka, T., 2022. Fenofibrate nano-eyedrops ameliorate retinal blood flow dysregulation and neurovascular coupling in type 2 diabetic mice. *Pharmaceutics* 14 (2), 384.

Hsu, Y.-J., Lin, C.-W., Cho, S.-L., Yang, W.-S., Yang, C.-M., Yang, C.-H., 2020. Protective effect of fenofibrate on oxidative stress-induced apoptosis in retinal–choroidal vascular endothelial cells: implication for diabetic retinopathy treatment. *Antioxidants* 9 (8), 712.

Huang, L., Liang, W., Zhou, K., Wassel, R.A., Ridge, Z.D., Ma, J.-X., Wang, B., 2021. Therapeutic effects of fenofibrate nano-emulsion eye drops on retinal vascular leakage and neovascularization. *Biology (Basel)*. 10 (12), 1328.

Ibáñez, C., Acuña, T., Quintanilla, M.E., Pérez-Reytor, D., Morales, P., Karahanian, E., 2023. Fenofibrate decreases ethanol-induced neuroinflammation and oxidative stress and reduces alcohol relapse in rats by a PPAR-α-dependent mechanism. *Antioxidants (Basel, Switzerland)* 12. https://doi.org/10.3390/antiox12091758.

Jagdale, S.K., Dehghan, M.H., Paul, N.S., 2019. Enhancement of dissolution of fenofibrate using complexation with hydroxy propyl β-cyclodextrin. *Turkish J. Pharm. Sci.* 16 (1), 48–53. https://doi.org/10.4274/tjps.60490.

Jansook, P., Loftsson, T., 2022. Self-assembled γ-cyclodextrin as nanocarriers for enhanced ocular drug bioavailability. *Int. J. Pharm.* 618, 121654.

Jansook, P., Pichayakorn, W., Muankaew, C., Loftsson, T., 2016. Cyclodextrin–poloxamer aggregates as nanocarriers in eye drop formulations: dexamethasone and amphotericin B. *Drug Dev. Ind. Pharm.* 42 (9), 1446–1454.

Kelly, S.J., Hirani, A., Shahidadpury, V., Solanki, A., Halasz, K., Varghese Gupta, S., Madow, B., Sutariya, V., 2018. Aflibercept nanoformulation inhibits VEGF expression in ocular in vitro model: A preliminary report. *Biomedicines* 6 (3), 92.

Khin, S.Y., Soe, H.M.S.H., Chansriniyom, C., Pornputtapong, N., Asasutjarit, R., Loftsson, T., Jansook, P., 2022. Development of fenofibrate/randomly methylated β-cyclodextrin-loaded eudragit® RL 100 nanoparticles for ocular delivery. *Molecules* 27 (15), 4755.

Krawczyk-Santos, A.P., Marreto, R.N., Concheiro, A., Alvarez-Lorenzo, C., Taveira, S.F., 2022. Poly (Pseudo) rotaxanes formed by mixed micelles and α-cyclodextrin enhance terbinafine nail permeation to deeper layers. *Int. J. Pharm. X* 4, 100118.

Lee, H.W., Kang, W.Y., Jung, W., Gwon, M.-R., Cho, K., Yang, D.H., Yoon, Y.-R., Seong, S. J., 2020. Evaluation of the pharmacokinetic drug–drug interaction between micronized fenofibrate and pitavastatin in healthy volunteers. *Pharmaceutics* 12 (9), 869.

Lorenzo-Veiga, B., Sigurdsson, H.H., Loftsson, T., Alvarez-Lorenzo, C., 2019. Cyclodextrin–amphiphilic copolymer supramolecular assemblies for the ocular delivery of natamycin. *Nanomaterials* 9 (5). https://doi.org/10.3390/nano9050745.

Lynnerup, J.T., Eriksen, J.B., Bauer-Brandl, A., Holsæter, A.M., Brandl, M., 2023. Insight into the Mechanism behind Oral Bioavailability-Enhancement by Nanosuspensions through Combined Dissolution/Permeation Studies. *Eur. J. Pharm. Sci.* 184, 106417.

Mahesh, M.B., Shrikrushna, A.S., Ganesh, S.T., 2020. Enhancement of solubility and dissolution rate of fenofibrate using β-cyclodextrin. *Innov. Pharm. Pharmacother.* 8 (3).

Nabih Maria, D., Mishra, R.S., Wang, L., Helmy Abd-Elgawad, A.-E., Abd-Elazeem Soliman, O., Salah El-Dahan, M., Jablonski, M.M., 2017. Water-soluble complex of curcumin with cyclodextrins: enhanced physical properties for ocular drug delivery. *Curr. Drug Deliv.* 14 (6), 875–886.

Nedelcu, A., Olteanu, A.-A., Constantinescu, I.C., Florea, M., Stănescu, L.-M., Bărbuceanu, Ş.F., Aramă, C.-C., 2022. Studies on the effects of inclusion complexation of fenofibrate with EPI-NS vs. β-CD and some of its substituted derivatives. *Farmacia* 70 (5).

Olsen, T.W., Sanderson, S., Feng, X., Hubbard, W.C., 2002. Porcine sclera: Thickness and surface area. *Invest. Ophthalmol. Vis. Sci.* 43 (8), 2529–2532.

Öztürk, K., Arslan, F.B., Öztürk, S.C., Çalış, S., 2022. Mixed micelles formulation for carvedilol delivery: In-vitro characterization and in-vivo evaluation. *Int. J. Pharm.* 611, 121294.

Pandit, J., Chaudhary, N., Emad, N.A., Ahmad, S., Solanki, P., Aqil, M., Sultana, Y., Solanki, P., 2023. Fenofibrate loaded nanofibers based thermo-responsive gel for ocular delivery: Formulation development, characterization and in vitro toxicity study. *J. Drug Deliv. Sci. Technol.* 89, 104935.

Patil, A., Lakhani, P., Taskar, P., Wu, K.-W., Sweeney, C., Avula, B., Wang, Y.-H., Khan, I. A., Majumdar, S., 2018. Formulation development, optimization, and in vitro–in vivo characterization of natamycin-loaded pegylated nano-lipid carriers for ocular applications. *J. Pharm. Sci.* 107 (8), 2160–2171.

Pecora, R., 2000. Dynamic light scattering measurement of nanometer particles in liquids. *J. Nanoparticle Res.* 2, 123–131.

Pepić, I., Hafner, A., Lovrić, J., Pirkić, B., Filipović-Grččić, J., 2010. A nonionic surfactant/chitosan micelle system in an innovative eye drop formulation. *J. Pharm. Sci.* 99 (10), 4317–4325. https://doi.org/10.1002/jps.22137.

Pescina, S., Govoni, P., Potenza, A., Padula, C., Santi, P., Nicoli, S., 2015. Development of a convenient ex vivo model for the study of the transcorneal permeation of drugs: histological and permeability evaluation. *J. Pharm. Sci.* 104 (1), 63–71. https://doi.org/10.1002/jps.24231.

Pescina, S., Grolli Lucca, L., Govoni, P., Padula, C., Del Favero, E., Cantù, L., Santi, P., Nicoli, S., 2019. Ex vivo conjunctival retention and transconjunctival transport of poorly soluble drugs using polymeric micelles. *Pharmaceutics* 11 (9), 476.

Pescina, S., Sonvico, F., Clementino, A., Padula, C., Santi, P., Nicoli, S., 2021. Preliminary investigation on simvastatin-loaded polymeric micelles in view of the treatment of the back of the eye. *Pharmaceutics*. https://doi.org/10.3390/pharmaceutics13060855.

Phan, C.-M., Ross, M., Fahmy, K., McEwen, B., Hofmann, I., Chan, V.W.Y., Clark-Baba, C., Jones, L., 2023. Evaluating viscosity and tear breakup time of contemporary commercial ocular lubricants on an in vitro eye model. *Transl. Vis. Sci. Technol.* 12 (6), 29. https://doi.org/10.1167/tvst.12.6.29.

Pignatello, R., Corsaro, R., Bonaccorso, A., Zingale, E., Carbone, C., Musumeci, T., 2022. Soluplus® polymeric nanomicelles improve solubility of BCS-Class II drugs. *Drug Deliv. Transl. Res.* 12 (8), 1991–2006.

Qiu, F., Matlock, G., Chen, Q., Zhou, K., Du, Y., Wang, X., Ma, J.-X., 2017. Therapeutic effects of PPARα agonist on ocular neovascularization in models recapitulating neovascular age-related macular degeneration. *Invest. Ophthalmol. vis. Sci.* 58 (12), 5065–5075.

Qiu, F., Meng, T., Chen, Q., Zhou, K., Shao, Y., Matlock, G., Ma, X., Wu, W., Du, Y., Wang, X., Deng, G., 2019. Fenofibrate-loaded biodegradable nanoparticles for the treatment of experimental diabetic retinopathy and neovascular age-related macular degeneration. Molecular pharmaceutics 16 (5), 1958–1970. https://doi.org/10.1021/acs.molpharmaceut.8b01319.

Rasoanirina, B.N.V., Lassoued, M.A., Kamoun, A., Bahloul, B., Miladi, K., Sfar, S., 2020. Voriconazole-loaded self-nanoemulsifying drug delivery system (SNEDDS) to improve transcorneal permeability. *Pharm. Dev. Technol.* 25 (6), 694–703.

Resende, A.P., Silva, B., Braz, B.S., Nunes, T., Gonçalves, L., Delgado, E., 2017. Ex vivo permeation of erythropoietin through porcine conjunctiva, cornea, and sclera. *Drug Deliv. Transl. Res.* 7, 625–631.

Rusznyák, Á., Palicskó, M., Malanga, M., Fenyvesi, É., Szente, L., Váradi, J., Bácskay, I., Vecsernyés, M., Réti-Nagy, K.S., Vasvári, G., 2022. Cellular effects of cyclodextrins: studies on hela cells. *Molecules* 27 (5), 1589.

Santana, C.P., Matter, B.A., Patil, M.A., Silva-Cunha, A., Kompella, U.B., 2023. Corneal permeability and uptake of twenty-five drugs: species comparison and quantitative structure–permeability relationships. *Pharmaceutics* 15 (6), 1646.

Saokham, P., Muankaew, C., Jansook, P., Loftsson, T., 2018. Solubility of Cyclodextrins and Drug/Cyclodextrin Complexes. *Molecules* 23 (5), 1161.

Sayed, S., Elsayed, I., Ismail, M.M., 2018. Optimization of β-cyclodextrin consolidated micellar dispersion for promoting the transcorneal permeation of a practically insoluble drug. *Int. J. Pharm.* 549 (1–2), 249–260. https://doi.org/10.1016/j.ijpharm.2018.08.001.

Setapa, A., Ahmad, N., Mohd Mahali, S., Mohd Amin, M.C.I., 2020. Mathematical model for estimating parameters of swelling drug delivery devices in a two-phase release. *Polymers (Basel)*. 12 (12), 2921.

Shaikhullina, M., Khaliullina, A., Gimatdinov, R., Butakov, A., Chernov, V., Filippov, A., 2020. NMR relaxation and self-diffusion in aqueous micellar gels of pluronic F-127. *J. Mol. Liq.* 306, 112898.

Shamma, R.N., Basha, M., 2013. Soluplus®: A novel polymeric solubilizer for optimization of carvedilol solid dispersions: Formulation design and effect of method of preparation. *Powder Technol.* 237, 406–414.

Simões, S.M.N., Veiga, F., Ribeiro, A.C.F., Figueiras, A.R., Taboada, P., Concheiro, A., Alvarez-Lorenzo, C., 2014. Supramolecular gels of poly-α-cyclodextrin and PEO-based copolymers for controlled drug release. *Eur. J. Pharm. Biopharm.* 87 (3), 579–588.

Singh, M., Bharadwaj, S., Lee, K.E., Kang, S.G., 2020. Therapeutic Nanoemulsions in Ophthalmic Drug Administration: Concept in Formulations and Characterization Techniques for Ocular Drug Delivery. *J. Control. Release* 328, 895–916.

Sitovs, A., Mohylyuk, V., 2024. Ex vivo permeability study of poorly soluble drugs across gastrointestinal membranes: acceptor compartment media composition. *Drug Discov. Today* 29 (12), 104214. https://doi.org/10.1016/j.drudis.2024.104214.

Sousa, F., Cruz, A., Fonte, P., Pinto, I.M., Neves-Petersen, M.T., Sarmento, B., 2017. A new paradigm for antiangiogenic therapy through controlled release of bevacizumab from PLGA nanoparticles. *Sci. Rep.* 7 (1), 1–13.

Stetefeld, J., McKenna, S.A., Patel, T.R., 2016. Dynamic Light Scattering: A Practical Guide and Applications in Biomedical Sciences. *Biophys. Rev.* 8, 409–427.

Sun, C., Li, W., Ma, P., Li, Y., Zhu, Y., Zhang, H., Adu-Frimpong, M., Deng, W., Yu, J., Xu, X., 2020. Development of TPGS/F127/F68 mixed polymeric micelles: enhanced oral bioavailability and hepatoprotection of syringic acid against carbon tetrachloride-induced hepatotoxicity. *Food Chem. Toxicol.* 137, 111126.

Tao, Y., Han, J., Wang, X., Dou, H., 2013. Nano-formulation of paclitaxel by Vitamin E succinate functionalized pluronic micelles for enhanced encapsulation, stability and cytotoxicity. *Colloids Surfaces B Biointerfaces* 102, 604–610.

Tapia-Guerrero, Y.S., Del Prado-Audelo, M.L., Borbolla-Jiménez, F.V., Gomez, D.M.G., García-Aguirre, I., Colín-Castro, C.A., Morales-González, J.A., Leyva-Gómez, G., Magaña, J.J., 2020. Effect of UV and gamma irradiation sterilization processes in the properties of different polymeric nanoparticles for biomedical applications. Mater. (Basel, Switzerland) 13. https://doi.org/10.3390/ma13051090.

Toffoletto, N., Saramago, B., Serro, A.P., Chauhan, A., 2023. A physiology-based mathematical model to understand drug delivery from contact lenses to the back of the eye. *Pharm. Res.* 40 (8), 1939–1951.

Varela-Garcia, A., Concheiro, A., Alvarez-Lorenzo, C., 2018. Soluplus micelles for acyclovir ocular delivery: Formulation and cornea and sclera permeability. *Int. J. Pharm.* 552 (1), 39–47. https://doi.org/10.1016/j.ijpharm.2018.09.053.

Veit, J.G.S., Birru, B., Singh, R., Arrigali, E.M., Serban, M.A., 2022. An In Vitro Model for characterization of drug permeability across the tympanic membrane. *Pharmaceuticals (Basel)*. 15 (9). https://doi.org/10.3390/ph15091114.

Vivero-Lopez, M., Sparacino, C., Quelle-Regaldie, A., Sánchez, L., Candal, E., Barreiro-Iglesias, A., Huete-Toral, F., Carracedo, G., Otero, A., Concheiro, A., 2022. PluronicŪ/Casein micelles for ophthalmic delivery of resveratrol: in vitro, ex vivo, and in vivo tests. *Int. J. Pharm.* 628, 122281.

Wang, J., Liu, Q., Yang, L., Xia, X., Zhu, R., Chen, S., Wang, M., Cheng, L., Wu, X., Wang, S., 2017. Curcumin-Loaded TPGS/F127/P123 Mixed Polymeric Micelles for Cervical Cancer Therapy: Formulation, Characterization, and in Vitro and in Vivo Evaluation. *J. Biomed. Nanotechnol.* 13 (12), 1631–1646.

Wang, L., Zhou, M. Ben, Zhang, H., 2021. The emerging role of topical ocular drugs to target the posterior eye. *Ophthalmol. Ther.* 10 (3), 465–494.
Williams III, R.O., Mahaguna, V., Sriwongjanya, M., 1998. Characterization of an inclusion complex of cholesterol and hydroxypropyl-β-cyclodextrin. *Eur. J. Pharm. Biopharm.* 46 (3), 355–360.
Worakul, N., Robinson, J.R., 1997. Ocular pharmacokinetics/pharmacodynamics. *Eur. J. Pharm. Biopharm.* 44 (1), 71–83.
Yang, B., Yang, L.-J., Lin, J., Chen, Y., Liu, Y., 2009. Binding behaviors of scutellarin with α-, β-, γ-cyclodextrins and their derivatives. *J. Incl. Phenom. Macrocycl. Chem.* 64, 149–155.